Chemical Engineering Journal 469 (2023) 143991

Contents lists available at ScienceDirect

Chemical Engineering Journal

journal homepage: www.elsevier.com/locate/cej

Tuning functional ionic deep eutectic solvents as green sorbents and catalysts for highly efficient capture and transformation of CO_2 to quinazoline-2,4(1*H*,3*H*)-dione and its derivatives

Guokai Cui [a], Yisha Xu [a], Daqing Hu [b], Ying Zhou [a], Chunliang Ge [b], Huayan Liu [a], Wenyang Fan [b], Zekai Zhang [a], Biao Chen [b], Quanli Ke [a], Yaoji Chen [b], Bing Zhou [a], Wei Zhang [b], Ruina Zhang [a], Hanfeng Lu [a,*]

[a] *Innovation Team of Air Pollution Control, Institute of Catalytic Reaction Engineering, College of Chemical Engineering, Zhejiang University of Technology, Hangzhou 310014, China*

[b] *Zhejiang Tiandi Environmental Protection Technology Co., Ltd., Hangzhou 310012, China*

ARTICLE INFO

Keywords:
Deep eutectic solvent
CO_2 utilization
Ionic liquid
CCUS
Green solvent

ABSTRACT

A series of functional ionic deep eutectic solvents (iDESs) containing pyridinolate anions were reported as green sorbents, solvents, and catalysts for highly efficient capture and transformation of CO_2 to quinazoline-2,4(1*H*,3*H*)-dione and its derivatives at mild conditions *via* tuning the structures of iDESs. Physical properties, such as density and viscosity, as well as flow activation energy and thermal expansion coefficient, were systematically investigated. Effects of the partial pressure of CO_2 and the absorption temperature on the CO_2 absorption capacity using these functional iDESs as sorbents were studied, and the different absorption mechanisms, including carbamate and carbonate pathways, were analyzed by FT-IR and ^{13}C NMR spectroscopy. Additionally, thermodynamics analysis of CO_2 absorption was performed according to the chemical reaction mechanism, and K^0,$\Delta_r G^0$m), $\Delta_r H^0$m, and $\Delta_r S^0$m were calculated. Furthermore, the effects of cations, anions, HBDs, reaction temperature, and the molar ratio of catalyst to substrate ($n_{Cat.}/n_{Sub.}$) on CO_2 conversion were systematically studied, and excellent isolated yield of up to 97.1% at mild conditions could be obtained with only 0.25 equiv. DES as the solvent as well as the sorbent and the catalyst. Plausible "simultaneous CO_2 activation and substrate activation" reaction mechanism of capture and transformation of CO_2 to quinazoline-2,4(1*H*,3*H*)-diones by [N_{2222}][4-PyO]/DMSO (1:4) was verified by the spectra of FT-IR and based on previous reports. To the best of our knowledge, these are the first examples of tuning functional iDESs for the capture and transformation of CO_2 to quinazoline-2,4-(1*H*,3*H*)-dione and its derivatives with only 0.25 equiv. DES. The method may also open a door to obtain the high efficiency of capture and transformation of such gases as NO_x, SO_2, CO, H_2S, and CO_2 by functional DESs.

1. Introduction

Recently, a series of problems were triggered by the increase concentration of CO_2 in the atmosphere, such as the global greenhouse effect, the acidification of the oceans, and the extinction of the wildlife. Carbon capture utilization and storage (CCUS) is an efficient way to deal with the emission of CO_2.[1] Although aqueous monoethanolamine (30 wt%) process has been used in industry for CO_2 capture during these decades, high energy consumption and high solvent loss during regeneration promote the development of alternative CCUS technologies.[2]

It is now known that CO_2 is a non-toxic C1 resource and could act as a "–CO_2-" or "–CO-" block to form carbonates, carbamates, amides, *etc.* [3–5] Thereby, capture and transformation of CO_2 to various value-added fine-chemicals and fuels is an important way to deal with the emission of CO_2. Among these fine-chemicals, heterocyclic compounds such as quinazoline-2,4(1*H*,3*H*)-diones with multiple biological and pharmacological activities for production of Prazosin, Bunazosin, and Doxazosin has received much more attention.[6,7] The conventional routes for synthesis quinazoline-2,4(1*H*,3*H*)-dione and its derivatives, such as the anthranilic acid + urea route, the anthranilic acid +

* Corresponding author.
E-mail address: luhf@zjut.edu.cn (H. Lu).

https://doi.org/10.1016/j.cej.2023.143991
Received 11 April 2023; Received in revised form 29 May 2023; Accepted 6 June 2023
Available online 8 June 2023

potassium cyanate route, and the anthranilamide + phosgene route or the chlorosulfonyl isocyanate route with kinds of basic catalysts, have the drawbacks of toxic raw materials, harsh reaction conditions, by-products, and water waste. Thus, alternative methods for environmentally friendly transformation of CO_2 to quinazoline-2,4(1*H*,3*H*)-diones are highly desired.

In recent decades, two kinds of green and sustainable solvents, ionic liquids (ILs) and deep eutectic solvents (DESs), have received lots of attention with similar tunable physical–chemical properties, including very low vapor pressure, high thermal and chemical stability, high solubilization capacity for inorganic and organic compounds *via* selecting suitable cations and anions or hydrogen bond accepters (HBAs) and hydrogen bond donors (HBDs).[8–11] There are several functional ILs reported for transformation of CO_2 to quinazoline-2,4(1*H*,3*H*)-diones, such as alkoxide anions,[12] carboxylate anions,[13,14] azolate anions,[15,16] imide anions,[17,18] *etc*. However, disadvantages including high reaction temperature, high CO_2 pressures, high cost and viscosity of pure ILs with low solubility of substituted 2-aminobenzonitriles limited their use. For example, Liu *et al*. prepared succinimide-based[17], triazolium-based[16], and aminophenol-based[19] ILs, which could catalyze 2-aminobenzonitrile with atmospheric-pressure CO_2 with high yield, but the process required a large amount of catalyst. CO_2 conversion by DESs is a chance to overcome the aforementioned disadvantages.[20] Recently, except some non-ionic DESs,[21–23] a large amount of DESs were designed and developed during these two decades (2003 ~ 2023) from IL salts, such as cholinium salts, imidazolium salts, ammonium salts, guanidinium salts *etc*. as HBAs and kinds of other inorganics and organics, such as urea,[24,25] alkanolamines,[26,27] ethylene glycol (EG),[28,29] phenols,[30,31] H_2O,[32–34] succinonitrile (SN),[35–37] dimethyl sulfoxide (DMSO), zinc chloride ($ZnCl_2$),[38,39] *etc*. as HBDs at different molar ratios (Scheme 1). The DESs could be used as green solvents, sorbents, and catalysts, in the fields of gas capture,[40–43] extraction,[44–46] energy,[47,48] environment,[49–51] pharmaceutics and medicine.[52] To the best of our knowledge, there are kinds of DESs used for the transformation of CO_2 to cyclic carbonates[53–55] and only a DES for carbamates synthesis,[56] while no publications about the synthesis of quinazoline-2,4(1*H*,3*H*)-diones from CO_2 using functional iDESs (Scheme 2). Thus, developing functional iDESs with efficient capture and transformation of CO_2 to quinazoline-2,4(1*H*,3*H*)-diones is important to give another opportunity to CCUS.

Herein, this contribution shows a novel strategy for highly efficient synthesis of quinazoline-2,4(1*H*,3*H*)-diones under mild conditions *via* transformation of CO_2 by functional iDESs as green solvents, sorbents and catalysts has been developed through tuning the structures of hydrogen bond accepters (HBAs) and hydrogen bond donors (HBDs) (Scheme 3). The density and viscosity, two important physical properties, were determined at the temperatures in the range of 20 ~ 80 °C under atmospheric pressure. The performance of CO_2 capture was measured under different temperature and CO_2 partial pressure. The thermodynamic properties of CO_2 absorbed in pyridinolate-containing functional iDESs such as the changes of absorption Gibbs free energy, enthalpy and entropy were systematically analyzed. Performance of CO_2 conversion using these functional iDESs as the catalysts was also investigated under different conditions. Functional iDESs containing pyridinolate anions showed highly efficient capture and transformation of CO_2 to quinazoline-2,4(1*H*,3*H*)-diones with the isolated yields up to 92.9% as well as only 0.25 equiv. DES at mild conditions through "simultaneous CO_2 activation and substrate activation" reaction mechanism.

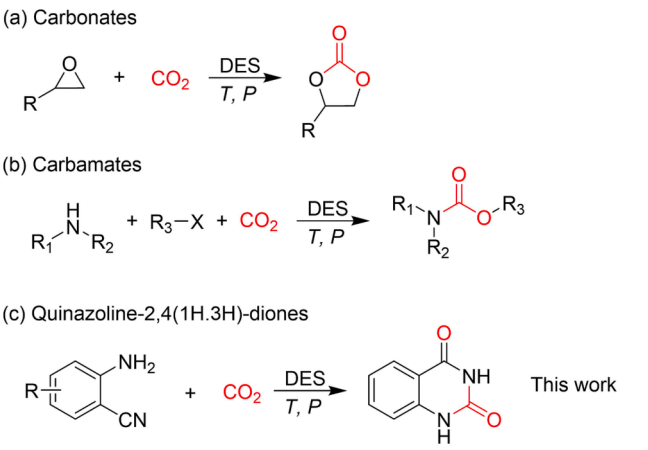

Scheme 2. CO_2 conversion by DESs to (a) carbonates, (b) carbamates, and (c) quinazoline-2,4(1*H*,3*H*)-diones.

2. Experimental methods

2.1. Materials

Cholinium hydroxide ([Ch][OH], 44% in water, CAS No. 123–41-1)

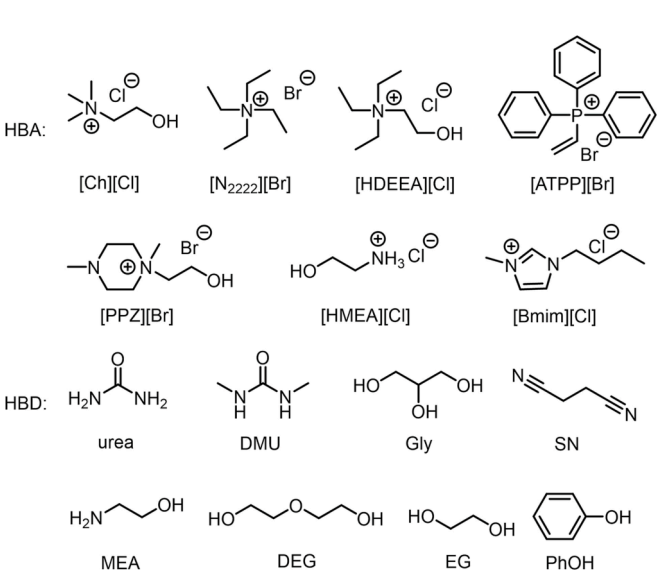

Scheme 1. Structures of typical HBAs and typical HBDs.

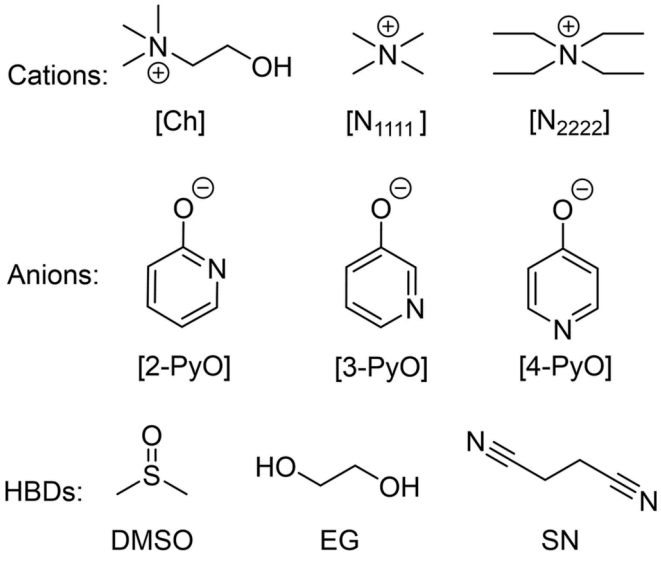

Scheme 3. Structures of cations, anions, and HBDs for the formation of functional iDESs.

and 4-hydroxypyridine (4-PyO, 97%, CAS No. 626–64-2) were obtained from Shanghai Aladdin Biochemical Technology Co., Ltd. 2-Aminobenzonitrile (ABN, 98%, CAS No. 1885–29-6), 2-amino-5-fluorobenzonitrile (5-F-ABN, 97%, CAS No. 61272–77-3), and succinonitrile (SN, 99%, CAS No. 110–61-2) were accessed from Shanghai Macklin Biochemical Co., Ltd. Tetramethylammonium hydroxide ([N_{1111}][OH], 25% in water, CAS No. 75–59-2), tetraethylamminonium hydroxide ([N_{2222}][OH], 25% in water, CAS No. 77–98-5), 2-amino-5-bromobenzonitrile (5-Br-ABN, 98%, CAS No. 39263–32-6), and 3-hydroxypyridine (3-PyO, 98%, CAS No. 109–00-2) were supplied from Shanghai Titan Scientific Co., Ltd. 2-Amino-4-methylbenzonitrile (4-CH_3-ABN, 98%, CAS No. 26830–96-6) and 2-amino-5-chlorobenzonitrile (5-Cl-ABN, 99.93%, CAS No. 5922–60-1) were approached from Shanghai Bide Pharmaceutical Technology Co., Ltd. Ethylene glycol (EG, 99%, CAS No. 107–21-1) and dimethyl sulfoxide (DMSO, 99.5%, CAS No. 67–68-5) were purchased from Sinopharm Chemical Reagent Co., Ltd. 2-Hydroxypyridine (2-PyO, 98%, CAS No. 72762–00-6) was procured from Meryer (Shanghai) Chemical Technology Co., Ltd. CO_2 (99.999%), CO_2 (5% CO_2, 95 % N_2), CO_2 (15% CO_2, 85 % N_2), and CO_2 (50% CO_2, 50 % N_2) were bought from Hangzhou Jingong Gas Co., Ltd.

2.2. Synthesis of functional iDESs

Functional iDESs were directly synthesized through stirring mixtures of ionic salts as HBAs and different HBDs with desired molar ratios of 1:3, 1:4 and 1:5 at 60 °C for 3 h. Typically, ([N_{2222}][4-PyO]) was prepared through neutralization reaction. Equimolar 4-PyO was added into [N_{2222}][OH] aqueous solution under dramatically stirring at room temperature for 12 h. Then, under the condition of reduced pressure, water was evaporated at 80 °C. In order to remove the possible trace of water, the obtained ILs were dried by freeze drying for 24 h. Other ionic salts, such as [N_{2222}][2-PyO], [N_{2222}][3-PyO], [N_{1111}][4-PyO], and [Ch][4-PyO]were synthesized in a similar way.

2.3. CO_2 absorption

Apparatus of CO_2 absorption by iDESs were shown in Scheme 4. With the flow rate of 60 ml min^{-1}, CO_2 with different concentrations was bubbled into about 1 g iDES at the desirable temperatures. The capacity was measured using an electronic balance with the accuracy of ± 0.0001 g at regular intervals and stopped when the absorption equilibrium was reached. The molecular mass of iDES was obtained by using equation $M_{iDES} = n_{HBA}M_{HBA} + n_{HBD}M_{HBD}$.

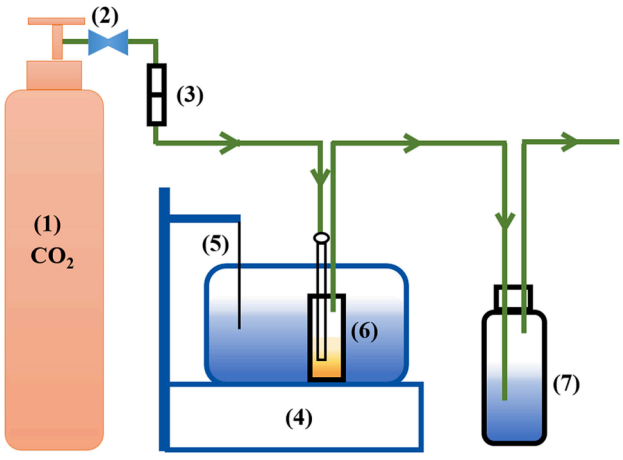

Scheme 4. Apparatus of CO_2 absorption by iDESs: (1) gas cylinder containing different concentration CO_2; (2) high pressure valve; (3) rotor flow meter; (4) magnetic stirrer; (5) thermocouple; (6) glass bottle filled with iDES; (7) off-gas absorption by NaOH.

2.4. Synthesis of quinazoline-2,4(1H,3H)-diones

Taking quinazoline-2,4(1*H*,3*H*)-dione obtained from ABN and CO_2 as an example, ABN (1 mmol) as the substrate and one of the iDESs (0.25 mmol) as the catalyst were sequentially added into a glass tube. CO_2 gas was slowly purged to exhaust the air inside the glass tube. Then the reaction container connected with a CO_2 balloon, and the reaction mixture was stirred at the desired temperatures for 24 h. After the reaction completed, 10 ml deionized water was added into the glass tube. Thus, the crude product was obtained through readily precipitation from the mixture, and it could be readily separated through centrifugation. Subsequently, after washing using deionized water and diethyl ether, the catalyst and unreacted ABN were removed. Finally, after dried at 60 °C for 24 h under vacuum, the mass of the product was weighted by an electronic balance (accuracy: ± 0.0001 g). The iDES catalyst for the next run could be recycled through evaporation of water.

2.5. Characterization

The chemical structures of these functional iDESs and CO_2-saturated iDESs were verified *via* NMR (Bruker 400 MHz) and FT-IR (VERTEX 70). DMSO-d_6 was selected as the solvent for NMR analyzing, and residual DMSO used as the reference. Densities of iDESs were carefully determined using a pycnometer at T = (293.2, 303.2, 313.2, 323.2, 333.2, 343.2 and 353.2) K under atmospheric pressure. Pycnometer was calibrated using ethylene glycol at temperatures mentioned above. The viscosities of the iDESs were measured by a Brookfield (DVNEXT-LV) viscometer at different temperatures. Karl Fisher titrator (870 KF Titrino plus) was used to determine the water contents of these iDESs, and the results were listed in Table S1 of Supporting Information. The melting points were measured on a TA Q2000 DSC in the range of − 80 ~ 40 °C at a heating rate of 10 °C min^{-1} under N_2 atmosphere, and the results were listed in Table S2 of Supporting Information. The melting points of the solids were obtained by capillary measurement. Thermal expansion coefficients were also calculated and listed in Table S3 of Supporting Information.

3. Results and discussion

3.1. Physical properties of functional iDESs

3.1.1. Density

The density (ρ) in g cm^{-3} and the viscosity (η) in mPa·s are two important physical properties of DESs. The densities of typical functional iDESs with different cations, anions, HBDs, and molar ratios of HBA: HBD were measured and the results were showed in Table 1.

To study the relationship of density *vs* temperature, the linear equation $\ln\rho = a + b\,T$ was used, where a and b are fitting parameters, and their values were collected in Table 2 ($R^2 > 0.99$), indicating the density decreased linearly with the increasing temperature for these functional iDESs (Fig. 1). Besides, the density of typical iDES was affected by cations, anions, HBDs, and molar ratios of HBA: HBD. For [Ch][4-PyO]/DMSO (1:4), [N_{1111}][4-PyO]/DMSO (1:4) and [N_{2222}][4-PyO]/DMSO (1:4) with different cations, the density of former is higher than that of latter at same temperature, due to the increased interaction between anion and cation containing short chain and hydroxyl group. For example, the densities of [Ch][4-PyO]/DMSO (1:4), [N_{1111}][4-PyO]/DMSO (1:4) and [N_{2222}][4-PyO]/DMSO (1:4) at 30 °C were 1.1101, 1.0875, and 1.0731 g cm^{-3}, respectively. For [N_{2222}][3-PyO]/DMSO (1:4), [N_{2222}][4-PyO]/DMSO (1:4) and [N_{2222}][2-PyO]/DMSO (1:4) with different anions, the measured density data at each temperature were very close, indicating that the anions have a less effect on the density of the DESs. Additionally, For [N_{2222}][4-PyO]/EG (1:4) and [N_{2222}][4-PyO]/SN (1:4), the density of former with strong hydrogen bonds is higher than that of latter at same temperature. For [N_{2222}][4-PyO]/DMSO (1:4), there is a rapid decrease in density with the

Table 1
Density (ρ) in g cm^{-3} and the viscosity (η) in mPa·s of typical functional iDESs.

iDES	Property	T (K) 293.2	303.2	313.2	323.2	333.2	343.2	353.2
[Ch][4-PyO]/DMSO (1:4)	ρ	1.1191	1.1101	1.1011	1.0926	1.0849	1.0750	1.0651
	η	18.91	12.81	9.12	6.79	5.41	4.35	3.53
[N_{2222}][4-PyO]/DMSO (1:4)	ρ	—	1.0731	1.0661	1.0569	1.0491	1.0419	1.0331
	η	—	9.20	6.50	4.87	4.06	3.25	2.56
[N_{1111}][4-PyO]/DMSO (1:4)	ρ	1.0965	1.0875	1.0785	1.0688	1.0602	1.0505	1.0425
	η	11.20	7.91	5.90	4.66	3.85	3.07	2.62
[N_{2222}][3-PyO]/DMSO (1:4)	ρ	1.0837	1.0757	1.0677	1.0584	1.0526	1.0422	1.0357
	η	11.93	8.38	6.15	4.83	3.77	3.05	2.35
[N_{2222}][2-PyO]/DMSO (1:4)	ρ	1.0721	1.0661	1.0601	1.0542	1.0486	1.0422	1.0361
	η	10.56	7.43	5.56	4.34	3.43	2.82	2.33
[N_{2222}][4-PyO]/SN (1:4)	ρ	1.0575	1.0515	1.0455	1.0407	1.0346	1.0292	1.0215
	η	257.10	122.10	65.50	38.58	24.62	17.04	12.32
[N_{2222}][4-PyO]/EG (1:4)	ρ	1.0769	1.0719	1.0669	1.0599	1.0545	1.0491	1.0449
	η	112.50	63.15	38.22	24.53	17.37	12.88	9.50
[N_{2222}][4-PyO]/DMSO (1:3)	ρ	—	—	1.0618	1.0546	1.0452	1.0372	1.0298
	η	—	—	8.99	6.94	5.12	4.13	3.36
[N_{2222}][4-PyO]/DMSO (1:5)	ρ	1.0830	1.0760	1.0670	1.0592	1.0511	1.0440	1.0370
	η	11.43	7.76	5.67	4.17	3.10	2.53	2.10

Table 2
Fitting parameters for equations $\ln\rho = a + bT$ and $\ln\eta = \ln\eta_0 + E_\eta/(RT)$.

iDES	Parameters for $\ln\rho = a + bT$			Parameters for $\ln\eta = \ln\eta_0 + E_\eta/(RT)$		
	a	b [$\times10^4$]	R^2	η_0[$\times10^6$]	E_η	R^2
[Ch][4-PyO]/DMSO (1:4)	0.351	−8.126	0.999	1002.338	23.836	0.995
[N_{2222}][4-PyO]/DMSO (1:4)	0.301	−7.603	0.999	1387.572	22.063	0.995
[N_{1111}][4-PyO]/DMSO (1:4)	0.341	−8.495	0.999	2233.802	20.621	0.995
[N_{2222}][3-PyO]/DMSO (1:4)	0.304	−7.624	0.998	1017.273	22.749	0.998
[N_{2222}][2-PyO]/DMSO (1:4)	0.236	−5.668	0.999	1504.101	21.461	0.997
[N_{2222}][4-PyO]/SN (1:4)	0.221	−5.619	0.997	4.119	43.390	0.992
[N_{2222}][4-PyO]/EG (1:4)	0.226	−5.188	0.997	54.953	35.172	0.994
[N_{2222}][4-PyO]/DMSO (1:3)	0.304	−7.782	0.998	1357.867	22.886	0.998
[N_{2222}][4-PyO]/DMSO (1:5)	0.295	−7.346	0.999	473.073	24.475	0.996

increasing temperature due to the strong polarity of DMSO. Furthermore, the molar ratio of HBA:HBD has a less effect on the density of [N_{2222}][4-PyO]/DMSO DESs. For example, the densities of [N_{2222}][4-PyO]/DMSO (1:5), [N_{2222}][4-PyO]/DMSO (1:4), and [N_{2222}][4-PyO]/DMSO (1:3) at 50 °C were 1.0592, 1.0569, and 1.0546 g cm^{-3}, respectively.

3.1.2. Viscosity

The viscosity of typical DESs was also affected by temperature, cations, anions, HBDs, and molar ratios of HBA: HBD, and the data were measured and showed in Fig. 2. The temperature has a great influence on the viscosity of the typical DESs. For example, the viscosity of [N_{2222}][4-PyO]/SN (1:4) decreased from 257.1 to 38.58 mPa·s with the increase of temperature from 20 to 50 °C. In addition, the relationship of viscosity *vs* temperature was correlated by the Arrhenius equation, $\ln\eta = \ln\eta_0 + E_\eta/(RT)$, where η_0 in mPa·s represents the pre-exponential constant, E_η in kJ mol^{-1} is the flow activation energy of iDES, and R = 8.314 J mol^{-1} K^{-1}. Fig. 2 shows the plotted ln η versus 1/T, and the values of parameters were also listed in Table 2 ($R^2 > 0.99$). The values of E_η for [N_{2222}][4-PyO]/SN (1:4), [N_{2222}][4-PyO]/EG (1:4), and [N_{2222}][4-PyO]/DMSO (1:4) were calculated to be 43.4, 35.2 and 22.1 kJ mol^{-1}, respectively.

3.1.3. Melting point

The melting points of these iDESs were also measured and listed in Table S2, and the corresponding DSC curves could be found in Fig. 3. It can be seen that the melting points of these iDESs were all below zero, in the range of − 35 ~ − 10 °C, except [N_{2222}][4-PyO]/SN (1:4) and [N_{2222}][4-PyO]/EG (1:4), melting points of which below − 80 °C. For comparison, the melting points of HBDs and HBAs were also tested. The melting points of DMSO, EG and SN were 18.4, −13, and 50 °C, respectively. Additionally, the melting points of [N_{2222}][4-PyO], [N_{2222}][3-PyO], [N_{2222}][2-PyO], and [N_{1111}][4-PyO] were 72, 40, 30 and 81 °C, respectively, while that of [Ch][4-PyO] was tested to be < − 18 °C. These results indicated that all these IL-based mixtures, except [Ch][4-PyO]/DMSO (1:4), were DESs, according to the definition of DESs.[57].

3.2. CO_2 absorption

3.2.1. Effects of different CO_2 partial pressures and absorption temperatures

Take [N_{2222}][4-PyO]/DMSO (1:4), [N_{2222}][4-PyO]/SN (1:4), and [N_{2222}][4-PyO]/EG (1:4) as the examples, the effect of different CO_2 partial pressures on CO_2 absorption capacity of typical functional iDESs, was studied and the results can be found in Fig. 4. CO_2 absorption capacities were decreased with the decrease of CO_2 partial pressure. For instance, the CO_2 absorption capacity of [N_{2222}][4-PyO]/DMSO (1:4) at 40 °C was decreased from 1.11 mol of CO_2 per mole of iDES under 1 bar to 0.77 mol of CO_2 per mole of iDES under 0.05 bar, indicating that captured CO_2 could be desorbed under low partial pressure as well as the capacity obtained under low concentration of CO_2 was mainly chemical.

The effect of absorption temperature on CO_2 capture capacity of typical functional iDESs was also investigated. CO_2 absorption capacity of each DES decreased with the increase of absorption temperature. CO_2 capacity of [N_{2222}][4-PyO]/DMSO (1:4) under 1 bar was decreased from 1.11 mol of CO_2 per mole of iDES at 40 °C to 0.85 mol of CO_2 per mole of iDES at 55 °C, indicating that the absorbed CO_2 can be released under high temperature.

In addition, the effect of structures of HBDs on the capture perforations of CO_2 was investigated. The results indicated that the order of CO_2 capture capacity was [N_{2222}][4-PyO]/DMSO (1:4) > [N_{2222}][4-PyO]/SN (1:4) > [N_{2222}][4-PyO]/EG (1:4) at the same conditions. For example, the capacities of CO_2 capture under 50 °C and 1 bar of [N_{2222}][4-PyO]/DMSO (1:4), [N_{2222}][4-PyO]/SN (1:4), and [N_{2222}][4-PyO]/EG (1:4) were 0.92, 0.77, and 0.73 mol of CO_2 per mole of iDES, respectively, indicating the tunable absorption of CO_2 by [N_{2222}][4-PyO]-containing DESs.

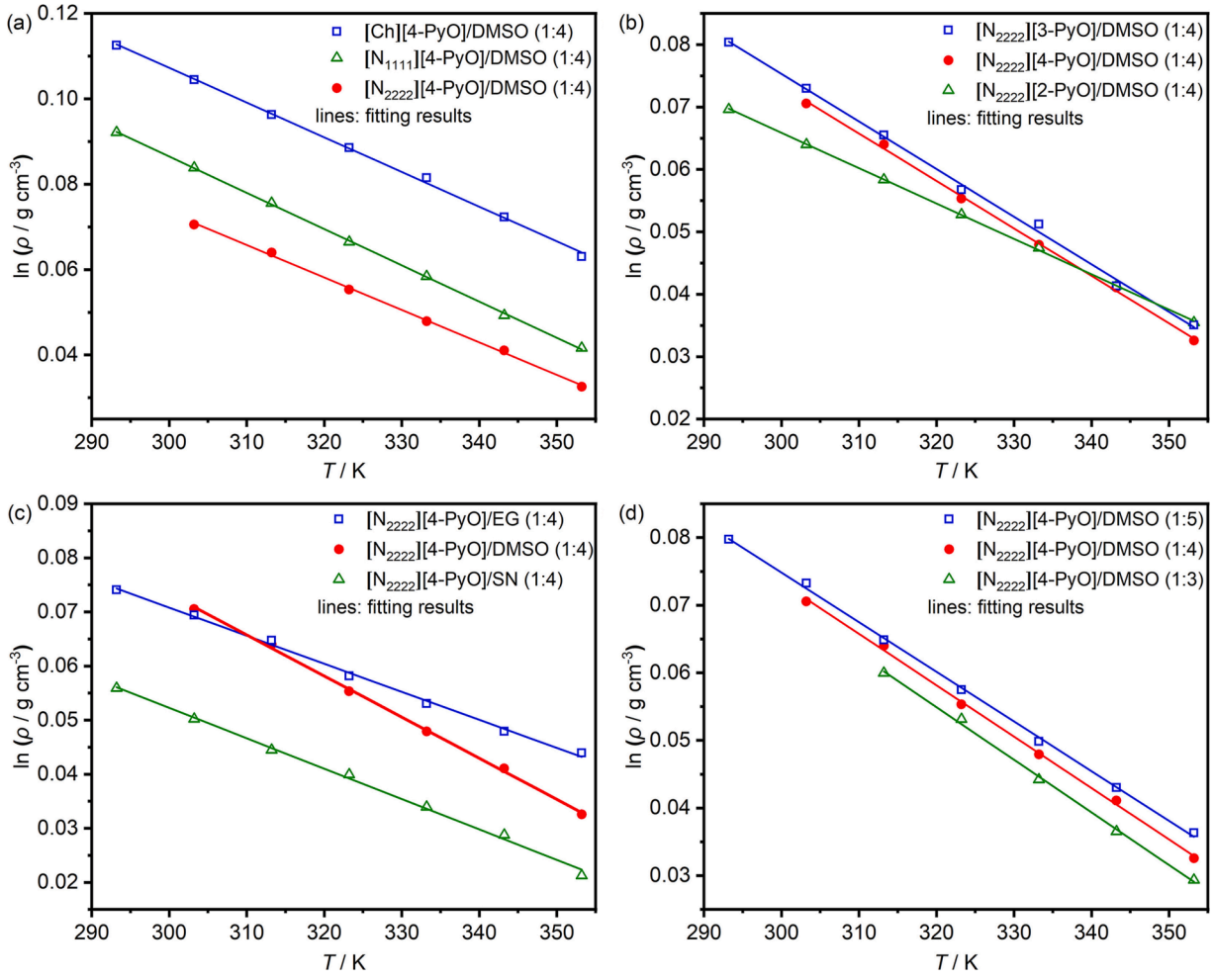

Fig. 1. Linear relationship of lnρ *vs T* for typical functional DESs with different cations (a), anions (b), HBDs (c), and molar ratios of HBA: HBD (d).

3.2.2. *Mechanism of CO_2 absorption*

To study the mechanisms of CO_2 absorptions in different iDESs, FT-IR and ^{13}C NMR spectroscopy of [N_{2222}][4-PyO]/DMSO (1:4) and [N_{2222}][4-PyO]/EG (1:4) before and after the absorption of CO_2 at 50 °C and 1 bar were analyzed (Fig. 5). Compared with the FT-IR spectrum of fresh [N_{2222}][4-PyO]/DMSO, two new peaks at 1635 and 1745 cm^{-1} can be found in the FT-IR spectrum of CO_2-saturated [N_{2222}][4-PyO]/DMSO (1:4) (Fig. 5a). According to the literature,[58] they can be assigned to the carbonyl carbons in carbonate (O···CO_2) and carbamate (N···CO_2), respectively. The formation of carbonate and carbamate could also be proved by ^{13}C NMR spectroscopy (Fig. 5b). In comparison with the ^{13}C NMR spectrum of the fresh DES [N_{2222}][4-PyO]/DMSO (1:4), two new chemical shifts at 145.3 and 158.2 ppm in the ^{13}C NMR spectrum of the CO_2 saturated iDES [N_{2222}][4-PyO]/DMSO (1:4) were produced, which could be attributed to the carbonyl carbons in carbamate (N···CO_2) and carbonate (O···CO_2), respectively. Because the capture capacity was readily lower than 1 mol of CO_2 per mole of [N_{2222}][4-PyO], it is safely to say that some [4-PyO] anions transformed to carbonate species while other [4-PyO] anions transformed to carbamate species after the interaction with CO_2 during the absorption of CO_2. When the capture capacity was found to be higher than 1 mol of CO_2 per mole of [N_{2222}][4-PyO], the complexes of [4-PyO] anions with two CO_2 were formed due to the multiple cooperative interactions.

In contrast, there is only one type of band at 1635 cm^{-1} in FT-IR spectrum of CO_2-saturated [N_{2222}][4-PyO]/EG (1:4), which could be attributed to the carbonyl carbon in carbonate (O···CO_2). Additionally, in comparison with the ^{13}C NMR spectrum of the fresh [N_{2222}][4-PyO]/EG (1:4), three new chemical shifts at 61.3, 65.7 and 156.9 ppm in the ^{13}C NMR spectrum of CO_2-saturated [N_{2222}][4-PyO]/EG (1:4) were produced, which could be attributed to two methylene carbons and a carbonate carbonyl carbon, respectively. According to the literature, [59] one of the hydroxyl groups in EG was dehydrogenation by [4-PyO] anion due to the anion's basicity, and neutral molecule 4-PyO was formed simultaneously. Based on previous reports [57,59,60] and the observed products, the mechanisms of CO_2 absorption by [N_{2222}][4-PyO]/EG (1:4) and [N_{2222}][4-PyO]/DMSO (1:4) are different, and the proposed plausible mechanisms could be illustrated in Scheme 5.

3.2.3. *Thermodynamics analysis of CO_2 absorption*

Thermodynamics analysis of CO_2 absorption by [N_{2222}][4-PyO]/DMSO (1:4), [N_{2222}][4-PyO]/SN (1:4), and [N_{2222}][4-PyO]/EG (1:4) was studied. It can be safely assumed that CO_2 capture at high temperature or low CO_2 partial pressure mainly through chemical interactions[40]. Thus, CO_2 absorptions were performed under 0.05 bar CO_2 at 313.2, 318.2, 323.2, and 328.2 K to discuss the thermodynamic properties. As aforementioned, single site absorption mechanisms (carbamate or carbonate) were followed during the CO_2 absorption by [N_{2222}][4-PyO]/DMSO (1:4), [N_{2222}][4-PyO]/SN (1:4), and [N_{2222}][4-PyO]/EG (1:4). Here, we do not distinguish between carbamate N site and carbonate O site, and study the average interaction or energy when we analyze the thermodynamic properties of CO_2 absorption by [N_{2222}][4-PyO]/DMSO (1:4) and [N_{2222}][4-PyO]/SN (1:4). Therefore, Equation (1) was used to describe these 1:1 chemical reactions:

$$CO_2 + DES \rightarrow DES\text{-}CO_2 \quad (1)$$

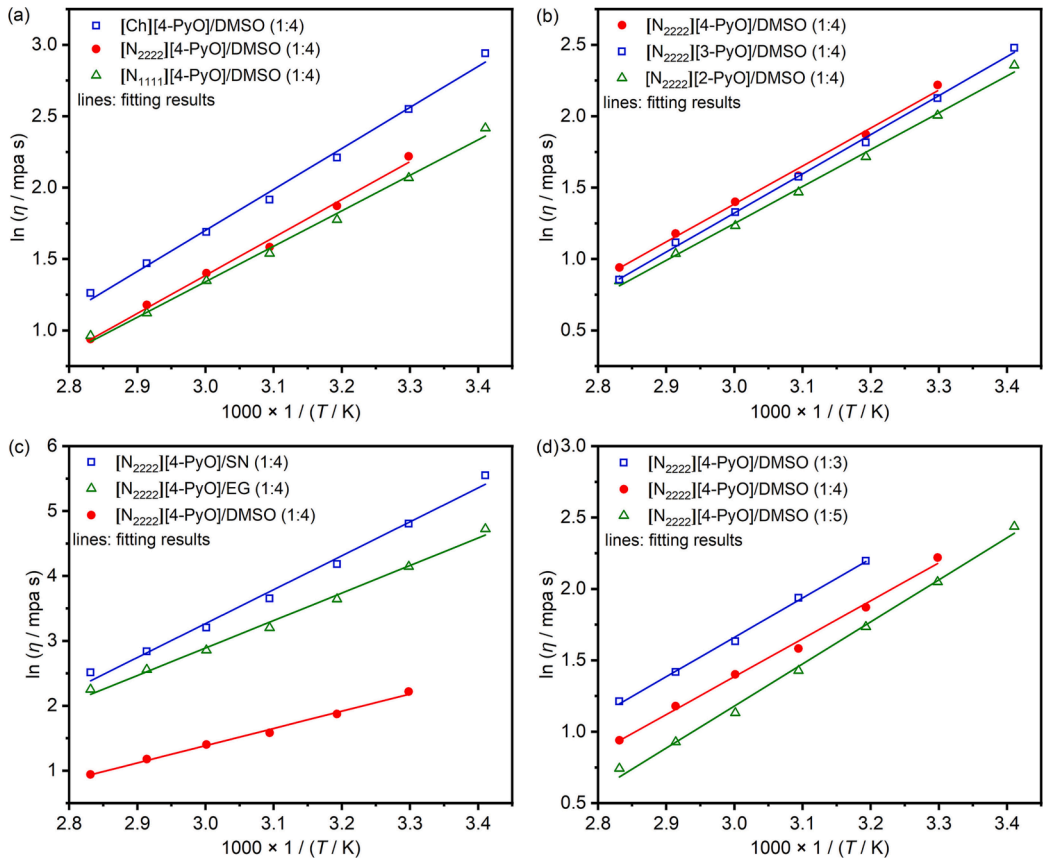

Fig. 2. Linear relationship of lnη *vs* 1/T for typical functional DESs with different cations (a), anions (b), HBDs (c), and molar ratios of HBA:HBD (d).

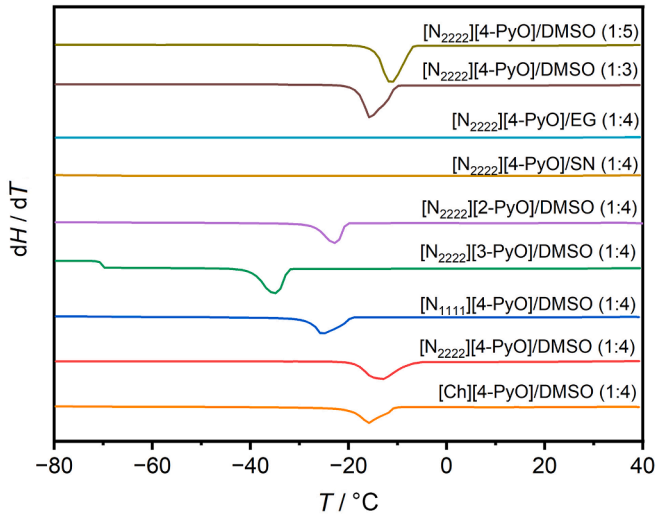

Fig. 3. DSC curves of iDESs for melting point measurement.

Chemical equilibrium constant, K^{θ}, in dimensionless of this reaction could be obtained through Equation (2):

$$K^{\theta} = \frac{Z_{\text{chem}}}{(1 - Z_{\text{chem}})P/P^{\theta}} \tag{2}$$

where Z_{chem} is the chemical absorption capacity in mol mol^{-1}. The calculated K^{θ} were collected in Table 3. K^{θ} values decreased with increasing temperature. For example, K^{θ} for CO_2 absorption by [N_{2222}][4-PyO]/DMSO (1:4) at 313.2, 318.2, 323.2, and 328.2 K were 66.96, 40.61, 22.55, and 18.46, respectively, indicating that low temperature is favorable for CO_2 absorption. In addition, the K^{θ} value at each temperature decreased with the order [N_{2222}][4-PyO]/DMSO (1:4) > [N_{2222}][4-PyO]/SN (1:4) > [N_{2222}][4-PyO]/EG (1:4), indicating that [N_{2222}][4-PyO]/DMSO (1:4) is favorable for CO_2 absorption.

In order to understand the thermodynamic driving force and evaluate the absorbents in practical application, the change of molar Gibbs free energy of the reaction ($\Delta_r G^{\theta}$m, in kJ mol^{-1}), the change of molar enthalpy of the reaction ($\Delta_r H^{\theta}$m, in kJ mol^{-1}), and the change of molar entropy of the reaction ($\Delta_r S^{\theta}$m, in J mol^{-1} K^{-1}) could be readily obtained by Equations (3–5) from chemical equilibrium constant K^{θ}, because of the quite narrow temperature range used in this contribution:

$$\Delta_r G^{\theta}_m = -RT\ln K^{\theta} \tag{3}$$

$$\Delta_r H^{\theta}_m = -R\left(\frac{\partial \ln K^{\theta}}{\partial(1/T)}\right) \tag{4}$$

$$\Delta_r S^{\theta}_m = \frac{\Delta_r H^{\theta}_m - \Delta_r G^{\theta}_m}{T} \tag{5}$$

The linear relationship of lnK^{θ} *vs* 1/T was showed in Fig. 6. The values of $\Delta_r G^{\theta}$m, $\Delta_r H^{\theta}$m and $\Delta_r S^{\theta}$m were listed in Table 3. The negative values of $\Delta_r G^{\theta}$m under the experimental conditions strongly indicated that the absorptions of CO_2 in DESs were favorable. The values of $\Delta_r H^{\theta}$m were also negative and $|\Delta_r H^{\theta}\text{m}| > 50$ kJ mol^{-1}, indicating the exothermic absorption process and the chemical interaction between CO_2 and DES. In addition, the negative $\Delta_r S^{\theta}$m values indicated that that the degree of disorder of the system becomes smaller due to the strong chemical interaction. Considering $\Delta_r H^{\theta}\text{m} < 0$, $\Delta_r S^{\theta}\text{m} < 0$, and $|\Delta_r H^{\theta}\text{m}| > |T\Delta_r S^{\theta}\text{m}|$, the sign of $\Delta_r G^{\theta}$m was determined by that of $\Delta_r H^{\theta}$m. Thus, the $\Delta_r H^{\theta}$m was predominant for the favorable 1:1 chemisorption of CO_2.

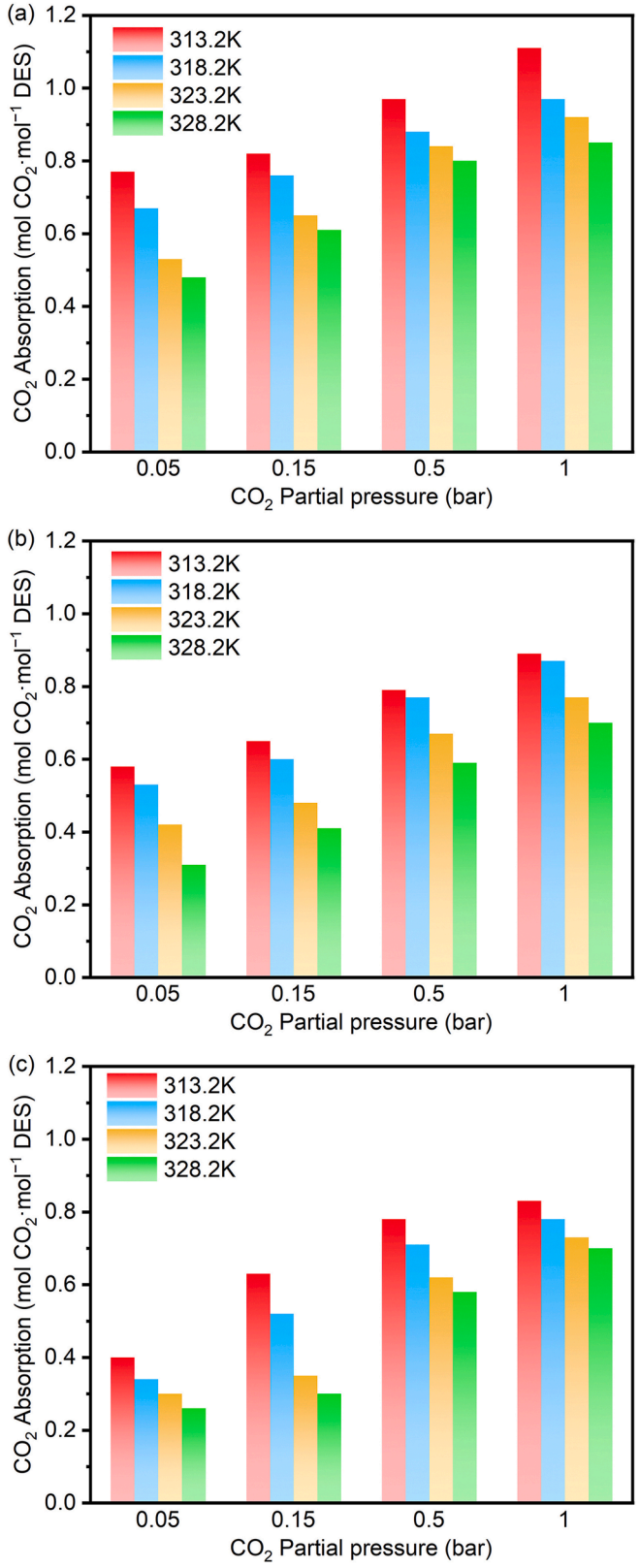

Fig. 4. CO_2 absorption by different DESs at different temperatures and CO_2 partial pressures. (a)[N_{2222}][4-PyO]/DMSO (1:4); (b)[N_{2222}][4-PyO]/SN (1:4); (c)[N_{2222}][4-PyO]/EG (1:4).

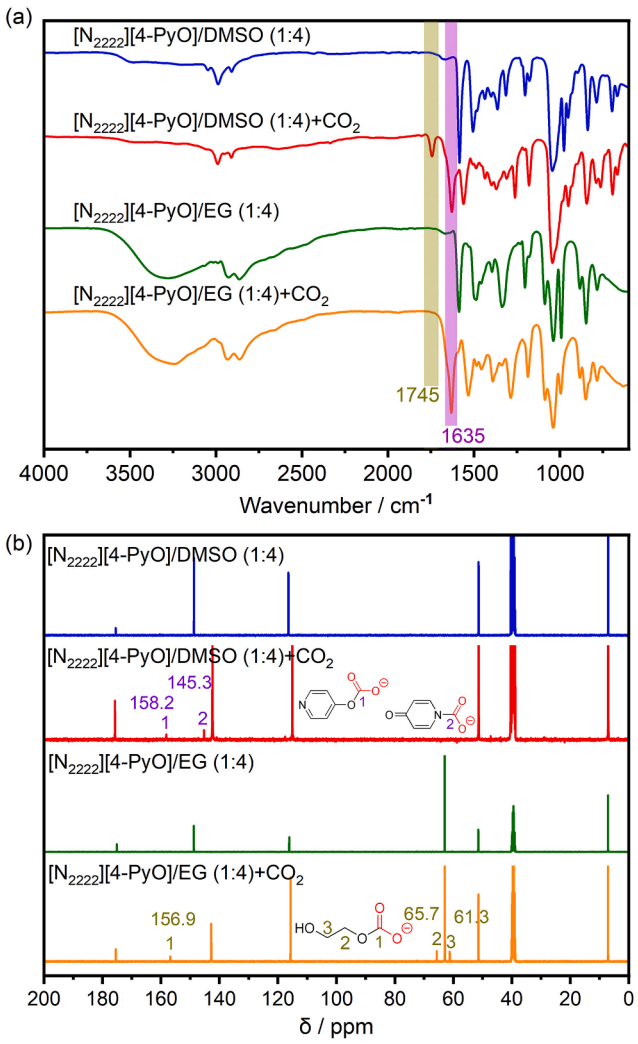

Fig. 5. (a) FT-IR and (b) ^{13}C NMR comparison of [N_{2222}][4-PyO]/DMSO (1:4) and [N_{2222}][4-PyO]/EG (1:4) before and after the absorption of CO_2 at 50 °C and 1 bar.

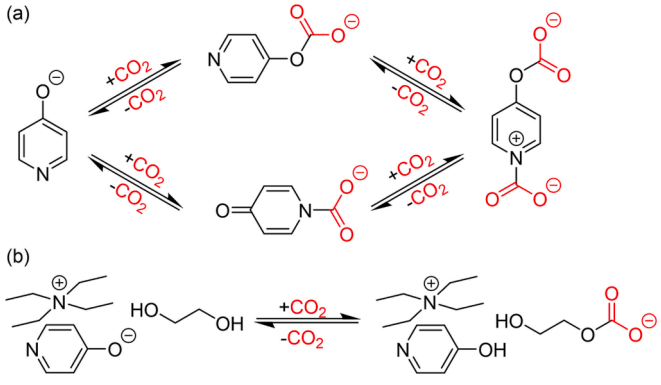

Scheme 5. Plausible mechanisms of CO_2 absorption by (a) [N_{2222}][4-PyO]/DMSO (1:4) and (b) [N_{2222}][4-PyO]/EG (1:4).

3.3. CO_2 conversion

3.3.1. Effects of cations, anions and HBDs on CO_2 conversion

These iDESs were used as green solvents, sorbents and catalysts for the transformation of CO_2 to quinazoline-2,4-(1*H*,3*H*)-dione and its

Table 3
Equilibrium constant (K^{θ}), change of molar Gibbs free energy of the reaction ($\Delta_r G\theta$ m), change of molar enthalpy of the reaction ($\Delta_r H\theta$ m), and change of molar entropy of the reaction ($\Delta_r S\theta$ m) for the CO_2 absorption by DESs.

DES	Property	T (K) 313.2	318.2	323.2	328.2
$[N_{2222}][4\text{-PyO}]$/DMSO (1:4)	K^{θ}	66.96	40.61	22.55	18.46
	R^2	0.971			
	$\Delta_r G^{\theta}$m (kJ mol^{-1})	−10.9	−9.8	−8.4	−8.0
	$\Delta_r H^{\theta}$m (kJ mol^{-1})	−76.3			
	$10^3\Delta_r S^{\theta}$m (kJ mol^{-1} K^{-1})	−208.8	−209.0	−210.1	−208.1
$[N_{2222}][4\text{-PyO}]$/SN (1:4)	K^{θ}	27.62	22.55	14.48	8.99
	R^2	0.967			
	$\Delta_r G^{\theta}$m (kJ mol^{-1})	−8.6	−8.2	−7.2	−6.0
	$\Delta_r H^{\theta}$m (kJ mol^{-1})	−65.0			
	$10^3\Delta_r S^{\theta}$m (kJ mol^{-1} K^{-1})	−180.1	−178.5	−178.8	−179.8
$[N_{2222}][4\text{-PyO}]$/EG (1:4)	K^{θ}	13.33	10.30	8.57	7.03
	R^2	0.996			
	$\Delta_r G^{\theta}$m (kJ mol^{-1})	−6.7	−6.2	−5.8	−5.3
	$\Delta_r H^{\theta}$m (kJ mol^{-1})	−35.5			
	$10^3\Delta_r S^{\theta}$m (kJ mol^{-1} K^{-1})	−92.0	−92.1	−91.9	−92.0

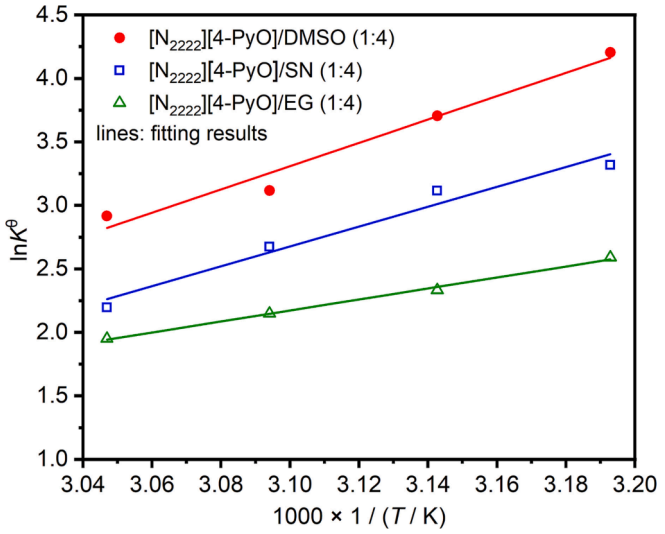

Fig. 6. Linear correlation between $\ln K^{\theta}$ and $1/T$.

derivatives. Choosing the cyclization of CO_2 and ABN to obtain quinazoline-2,4-(1*H*,3*H*)-dione as a model reaction, the effects of cations, anions as well as HBDs on CO_2 conversion were systematically studied, and the results are showed in Table 4.

The effect of cations of DESs on CO_2 conversion was first studied, and the results were showed in Entries 1, 2 and 5, Table 4. The order of isolated yields at 50 °C and 1 bar is $[N_{2222}][4\text{-PyO}]$/DMSO (1:4) > $[N_{1111}][4\text{-PyO}]$/DMSO (1:4) > 90% > [Ch][4-PyO]/DMSO (1:4), indicating that the cation of catalyst with long chains resulted in high yield because of the weaker interaction of cation···anion. Entries 3 ~ 6 illustrated the results of the effect of DMSO's dosage on CO_2 conversion. It can be found that the order of isolated yields at 50 °C and 1 bar is $[N_{2222}][4\text{-PyO}]$/DMSO (1:4) > 90% > $[N_{2222}][4\text{-PyO}]$/DMSO (1:5) > $[N_{2222}][4\text{-PyO}]$/DMSO (1:3) > 80% > $[N_{2222}][4\text{-PyO}]$ > 70%. When adding more DMSO as HBD, it promotes isolated yield. In addition, Entries 5, 7 and 8 showed the results of the effect of anion on CO_2 conversion. These anions have the difference in the position of N atom in the aromatic ring. It can be see that the order of isolated yields at 50 °C and 1 bar is $[N_{2222}][4\text{-PyO}]$/DMSO (1:4) > 90% > $[N_{2222}][3\text{-PyO}]$/DMSO (1:4) > $[N_{2222}][2\text{-PyO}]$/DMSO (1:4) > 70%. The highest isolated yield of 92.9% was obtained with $[N_{2222}][4\text{-PyO}]$/DMSO (1:4) as the catalyst probably due to the N site and O site on the opposite positions of [4-PyO] anion. Furthermore, the effect of HBDs, including DMSO, SN, and EG, on CO_2 conversion was investigated, and the order of isolated yields was $[N_{2222}][4\text{-PyO}]$/DMSO (1:4) > 90% > $[N_{2222}][4\text{-PyO}]$/SN (1:4) > 50% > $[N_{2222}][4\text{-PyO}]$/EG (1:4) > 30%, according to the results listed in Entries 5, 9 and 10. Clearly, the effect of HBDs is a key factor that has a significant impact on the isolated yields using DESs as the catalysts.

Table 4
The effects of cations, anions, and HBDs on CO_2 conversion by DESs as catalysts.[a]

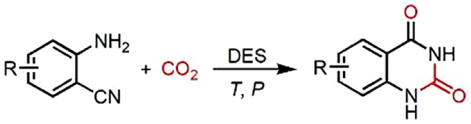

Entry	Catalyst	$n_{Cat.}/n_{Sub.}$	T (°C)	Isolated yield (%)
1	[Ch][4-PyO]/DMSO (1:4)	1:4	50	78.3
2	$[N_{1111}][4\text{-PyO}]$/DMSO (1:4)	1:4	50	91.2
3	$[N_{2222}][4\text{-PyO}]$	1:4	50	76.3
4	$[N_{2222}][4\text{-PyO}]$/DMSO (1:3)	1:4	50	84.5
5	$[N_{2222}][4\text{-PyO}]$/DMSO (1:4)	1:4	50	92.9
6	$[N_{2222}][4\text{-PyO}]$/DMSO (1:5)	1:4	50	89.9
7	$[N_{2222}][3\text{-PyO}]$/DMSO (1:4)	1:4	50	75.8
8	$[N_{2222}][2\text{-PyO}]$/DMSO (1:4)	1:4	50	72.5
9	$[N_{2222}][4\text{-PyO}]$/SN (1:4)	1:4	50	59.0
10	$[N_{2222}][4\text{-PyO}]$/EG (1:4)	1:4	50	32.7
11	$[N_{2222}][4\text{-PyO}]$/EG (1:4)	1:1	50	58.8
12	$[N_{2222}][4\text{-PyO}]$/DMSO (1:4)	1:4	30	35.4
13	$[N_{2222}][4\text{-PyO}]$/DMSO (1:4)	1:4	80	93.6
14	$[N_{2222}][4\text{-PyO}]$/DMSO (1:4)	1:2	50	95.1
15	$[N_{2222}][4\text{-PyO}]$/DMSO (1:4)	1:1	50	96.3

[a] Reaction conditions: ABN 1 mmol, DES 0.25 mmol, reaction time 24 h, 1 bar CO_2 balloon.

Moreover, the effects of reaction temperature and the molar ratio of iDES catalyst to substrate ($n_{Cat.}/n_{Sub.}$) were also studied, and the results were listed in Table 4 too, using $[N_{2222}][4\text{-PyO}]$/DMSO (1:4) as the optimal catalyst. It can be seen from Entries 5, 12 and 13 that the isolated yields at 30, 50 and 80 °C were 35.4, 92.9, and 93.6%, respectively, indicating that the isolated yield increases with the increasing reaction temperature from 30 to 50 °C and remains steady when reaction temperature above 50 °C. The effect of $n_{Cat.}/n_{Sub.}$ such as 1:4, 1:2, and 1:1 was studied and the results were showed in Entries 5, 14 and 15 for $[N_{2222}][4\text{-PyO}]$/DMSO (1:4) and Entries 10 and 11 for $[N_{2222}][4\text{-PyO}]$/EG (1:4), respectively. The isolated yields at $n_{Cat.}/n_{Sub.}$ = 1:4, 1:2, and 1:1 for $[N_{2222}][4\text{-PyO}]$/DMSO (1:4) were 92.9, 95.1, and 96.3%, respectively, indicating that the isolated yield increased with the increasing $n_{Cat.}/n_{Sub.}$. However, the increasement of isolated yield was not significant for $[N_{2222}][4\text{-PyO}]$/DMSO (1:4). Interestingly, isolated yield was increased 80% for $[N_{2222}][4\text{-PyO}]$/EG (1:4) when $n_{Cat.}/n_{Sub.}$ increased from 1:4 to 1:1. Based on the above discussion, the optimal reaction conditions should be $n_{Cat.}/n_{Sub.}$ = 1:4 at 50 °C with $[N_{2222}][4\text{-PyO}]$/DMSO (1:4) as the catalyst.

3.3.2. *Mechanism of CO_2 conversion*

The mechanism of CO_2 conversion into quinazoline-2,4(1*H*,3*H*)-diones using iDES $[N_{2222}][4\text{-PyO}]$/DMSO (1:4) as the catalyst can be verified using FT-IR spectra. Fig. 7 showed the FT-IR spectra of CO_2 conversion processes using $[N_{2222}][4\text{-PyO}]$/DMSO with different molar ratios of HBA:HBD as the catalyst. As illustrated in the Fig. 7a, without DMSO, CN peak at 2213 cm^{-1} could still be detected after 24 h in FT-IR spectrum of reaction system using neat $[N_{2222}][4\text{-PyO}]$ as the catalyst. Thus, the results indicated that the substrate had not been completely

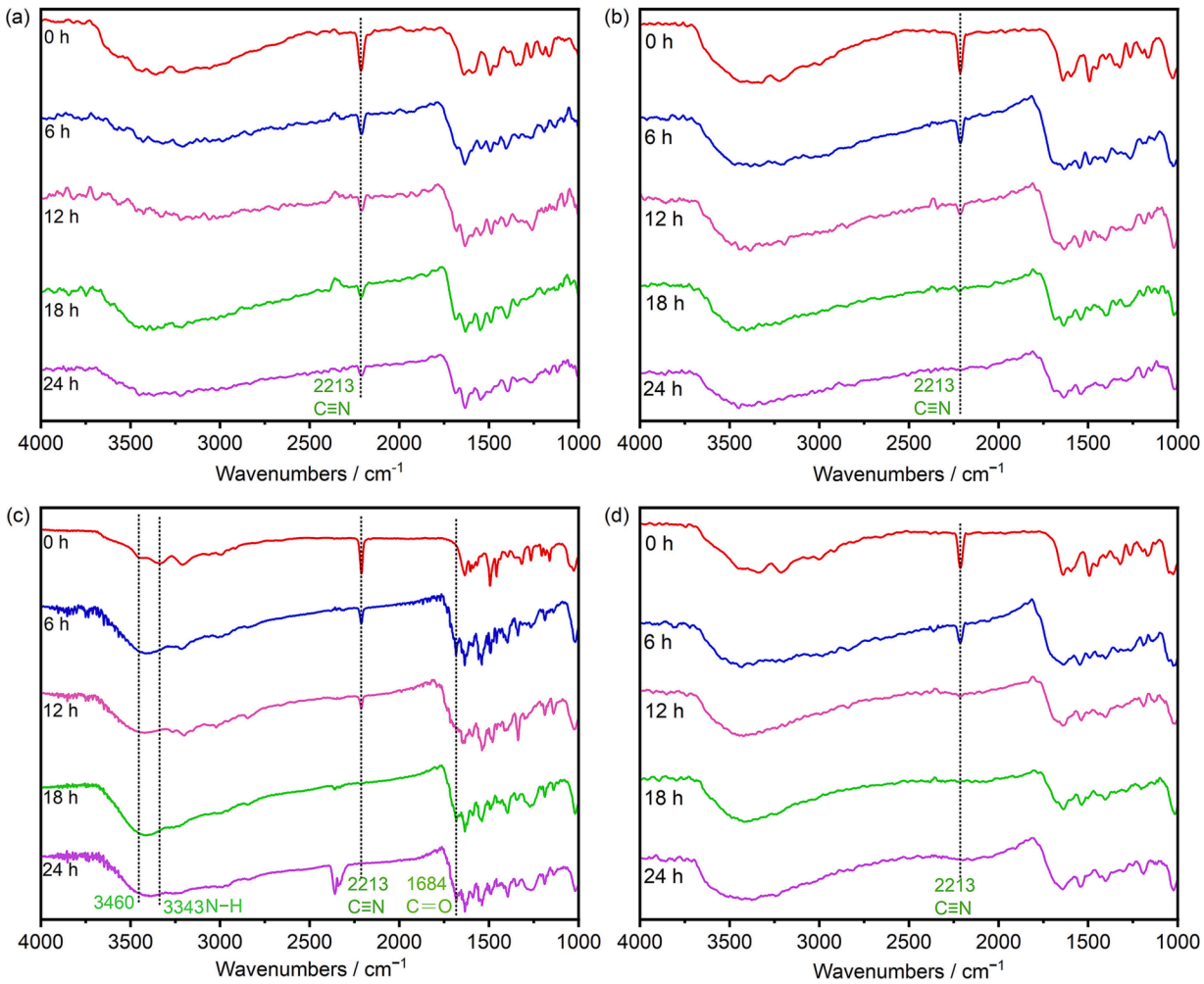

Fig. 7. FT-IR spectra of CO_2 react with ABN using (a) $[N_{2222}][4\text{-PyO}]$, (b) $[N_{2222}][4\text{-PyO}]$/DMSO (1:3), (c) $[N_{2222}][4\text{-PyO}]$/DMSO (1:4), and (d) $[N_{2222}][4\text{-PyO}]$/DMSO (1:5) as the catalyst at 50 ℃ and 1 bar CO_2.

transformed. On the contrary, with the increase of DMSO in reaction system, the CN peak of 2-aminobenzonitrile all disappeared after 24 h in $[N_{2222}][4\text{-PyO}]$/DMSO with different molar ratios of HBA:HBD as catalyst (Fig. 7b ~ d). It can be seen that the strength of N–H peaks of amino group at 3460 and 3343 cm^{-1} becomes weaker and broader with increasing reaction time. Simultaneously, strength of CN peak at 2213 cm^{-1} decreases gradually till it disappears with the increasing reaction time. In addition, another new peak at 1684 cm^{-1} during CO_2 conversion indicates the formation of C = O. Therefore, 2-aminobenzonitrile is successfully transformed to quinazoline-2,4(1*H*,3*H*)-dione. It can be safely concluded that, compared with neat IL, DMSO in these iDESs is beneficial for improving the isolated yield of product (Entries 3 ~ 6, Table 4).

In addition, the comparison of FT-IR and ^1H NMR spectra of neat ABN and ABN–$[N_{2222}][4\text{-PyO}]$/DMSO with different molar ratios of HBA:HBD were showed in Fig. 8. As the molar ratio of HBA:HBD increased, a new peak at 3337 cm^{-1} can be found in the FT-IR spectrum (Fig. 8a). According to the literature[18], they can be assigned to the formation of the NH···O = S hydrogen bond, which is attributed to the strong polarity of DMSO. Similarly, compared with the ^1H NMR spectrum of neat ABN, an obvious downfield shift of the 2-aminobenzonitrile NH_2 proton signal occurred in the ^1H NMR spectrum of ABN-$[N_{2222}][4\text{-PyO}]$ (Fig. 8b), suggesting the activation of ABN by $[N_{2222}][4\text{-PyO}]$ through hydrogen bonding. With the addition of DMSO, the chemical shift of the 2-aminobenzonitrile NH_2 proton signal gradually shifts to the up-field, due to the hydrogen bonds of NH_2···DMSO.

Furthermore, density functional theory (DFT) calculations at B3LYP/6–31G++(d,p) level with Gaussian 16 [61] were used to investigate the mechanism of CO_2 conversion by $[N_{2222}][4\text{-PyO}]$/DMSO. In the beginning, the interactions of $[4\text{-PyO}]\cdots CO_2$ were calculated, due to the key role of anion in CO_2 absorption by DESs. The optimized structures of [4-PyO]–CO_2 (N···CO_2) and [4-PyO]–CO_2 (O···CO_2) were shown in Scheme 6. It is shown that the intermolecular distances between N(or O) atom and C atom in two kinds of [4-PyO]–CO_2 were predicted to be 1.561 Å for N···C and 1.595 Å for O···C, respectively. The calculated O = C = O angles in [4-PyO]–CO_2 (N···CO_2) and [4-PyO]–CO_2 (O···CO_2) amount to 134.9 and 138.5°, indicating that there was a strong interaction between [4-PyO] and CO_2. The interactions of $[4\text{-PyO}]$/DMSO···CO_2 were also calculated. The results showed that the intermolecular distances of N···CO_2 and O···CO_2 as well as the calculated O = C = O angles both decreased in $[4\text{-PyO}]$/DMSO···CO_2 systems, indicating the more active CO_2 could be obtained in DESs than ILs, due to the cooperation (hydrogen bonds) between DMSO and CO_2.

DFT calculations were also used to analyze the effect of DMSO in CO_2 conversion by $[N_{2222}][4\text{-PyO}]$/DMSO, and the optimized structures of ABN, [PyO]–ABN and [PyO]–ABN–DMSO were shown in Scheme 7. It is shown that the calculated –NH_2 angles in ABN, [PyO]–ABN and [PyO]–ABN–DMSO amount to 115.5, 109.9 and 112.7°, indicating that there was a strong interaction between [4-PyO] and ABN while it was decreased in [4-PyO]/DMSO···ABN system. However, it should be noted that the molar ratio of ABN to [4-PyO] is only 1:0.25 in the reaction system, indicating the less interaction between $[4\text{-PyO}]_{0.25}$ and ABN.

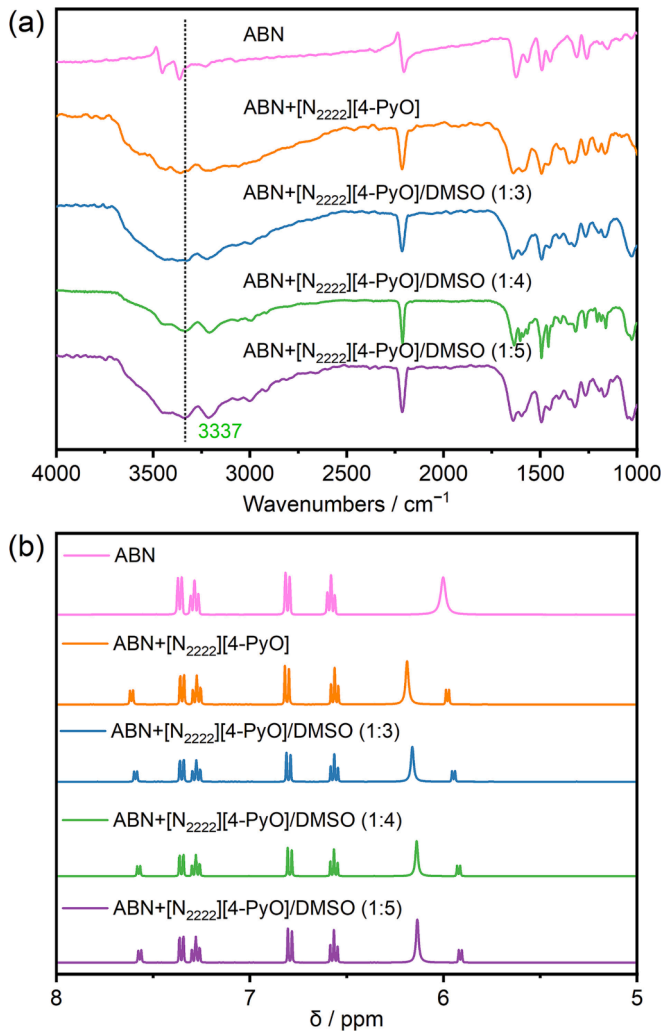

Fig. 8. (a) FT-IR and (b) ^{1}H NMR comparison of ABN and [N_{2222}][4-PyO]/DMSO with different molar ratios of HBA:HBD.

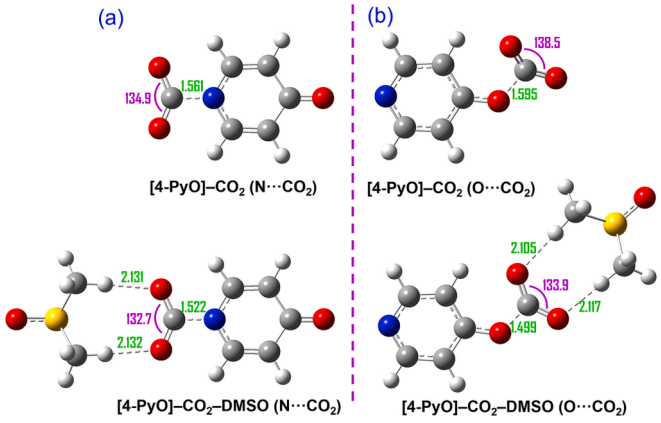

Scheme 6. Optimized structures of [4-PyO]–CO_2 complexes at B3LYP/6–31++G(d,p) level. (a) the N atom on the [4-PyO] anion with the closest CO_2 molecule; (b), the O atom on the [4-PyO] anion with the closest CO_2 molecule. Note that van der Waals radii (in Å) are 1.70 (C), 1.20 (H), 1.52 (O), 1.55 (N), 1.80 (S).[62].

Considering this situation, the added equimolar DMSO as HBD in reaction system resulted in that the intermolecular distance between H atom of NH_2 and O atom of DMSO was predicted to be 2.021 Å, corresponding

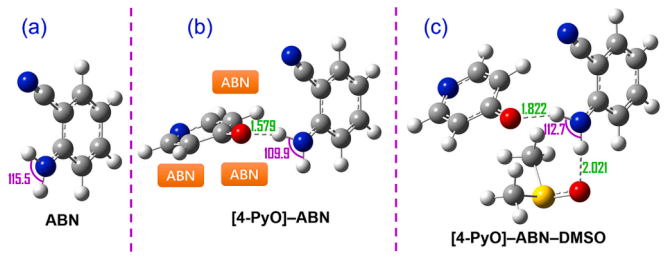

Scheme 7. Optimized structures of (a) ABN, (b) [PyO]–ABN and (c) [PyO]–ABN–DMSO complexes at B3LYP/6–31++G(d,p) level.

to a reduction of approximately 27% of the sum of the van der Waals radii of the two interacting atoms. Thus, the added NH_2···DMSO hydrogen bonding leading to the active ABN in CO_2 conversion.

Based on the previous reports [7,18] and the obtained product, the plausible mechanism of CO_2 conversion by [N_{2222}][4-PyO]/DMSO (1:4) could be proposed as described in Scheme 8. It is clear that [N_{2222}][4-PyO]/DMSO (1:4) can activate CO_2, forming carbamate or carbonate [X–CO_2] anions as active CO_2 species. At the same time, hydrogen bonds were formed between DMSO and [X–CO_2] anions. On the other hand, hydrogen bonds were formed between the N and O sites in [4-PyO] anion and the amino group in 2-aminobenzonitrile, due to the basicity of [4-PyO] anion. In addition, DMSO can also form hydrogen bond with the H atom in 2-aminobenzonitrile NH_2, which is beneficial for the [4-PyO] anion to remove H from 2-aminobenzonitrile. Simultaneously with CO_2 activation, negative charged active amino group –HN^- as well as neutral 4-PyO could be formed *via* simultaneous dehydrogenation. Later, high basic –HN^- nucleophilically attacks the C of CO_2 from active species [X–CO_2], resulting in the formation of the carbamate intermediate accompanied by the removal of [X] anion. Then, it transfers to cyclic carbonate intermediate *via* intramolecular nucleophilic cyclization. After proton transfer from –NH to –OH, the chemical bond OC–OH breaks to form an isocyanate intermediate, followed by the spontaneous intramolecular rearrangement. Finally, the quinazoline-2,4(1*H*,3*H*)-diones is obtained by proton transfer from neutral 4-PyO, and [4-PyO] anion is regenerated at the same time.

3.3.3. *Recycling of iDESs*

It is known that the cycle stability plays an essential role in catalysts' practical applications. In order to evaluate the cycle stability, the [N_{2222}][4-PyO]/DMSO (1:4), as an example, was reobtained through evaporation of water and reused as catalyst for the reaction of CO_2 and 2-aminobenzonitrile. The reaction was carried out at 50 °C and 1 bar CO_2. As shown in Fig. 9, after six cycles, the isolated yield of quinazoline-2,4(1*H*,3*H*)-dione is no obvious decrease, indicating that the catalysis activity of [N_{2222}][4-PyO]/DMSO (1:4) is maintained steadily. Therefore, this iDES is an efficient and outstanding catalyst.

3.3.4. *CO_2 conversion with different substituted 2-aminobenzonitriles*

CO_2 conversion with different substituted ABNs, such as 4-CH_3-ABN, 5-F-ABN, 5-Cl-ABN, and 5-Br-ABN, were also studied (Table 5). Order of isolated yields of products from halogen substituted ABNs was 5-F-ABN (97.1%) > 5-Cl-ABN (91.4%) > 5-Br-ABN (90.9%), due to the decreased electron-withdrawing ability. For example, F atom with the strongest electron-withdrawing ability reduced the electron density of benzene ring, leading to the strongest dehydrogenation of amino group in ABNs, resulting in the highest isolated yield. For comparison, the isolated yield of product from 4-CH_3-ABN was only 73.0%, due to the electro-donating ability of methyl. Thus, these results proved the plausible reaction mechanism.

4. Conclusions

In summary, a strategy for efficient capture and transformation of

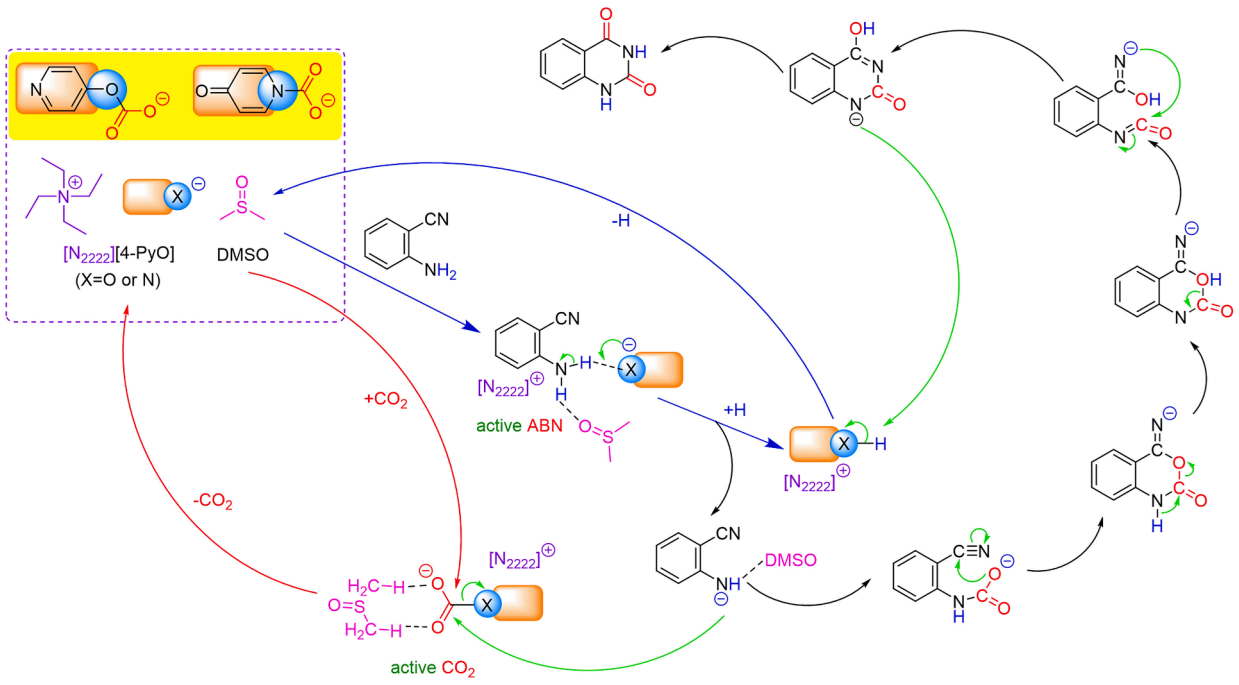

Scheme 8. Plausible reaction mechanism of CO_2 with ABN using iDES $[N_{2222}][4\text{-PyO}]$/DMSO (1:4).

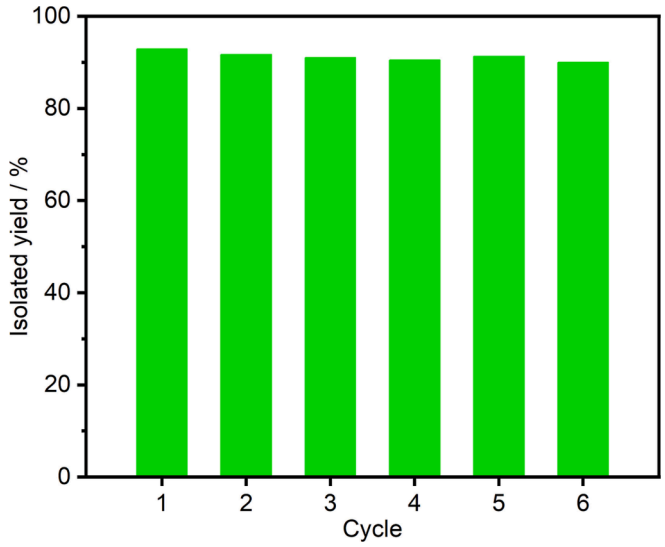

Fig. 9. Recycling stability of $[N_{2222}][4\text{-PyO}]$/DMSO (1:4) in the reaction of CO_2 and 2-aminobenzonitrile. Reaction conditions: ABN 1 mmol, DES 0.25 mmol, reaction time 24 h, reaction temperature 50 °C, 1 bar CO_2 balloon.

CO_2 to quinazoline-2,4(1*H*,3*H*)-diones by functional iDESs containing pyridinolate anions as green solvents, sorbents and catalysts under mild conditions has been developed *via* tuning the structures of DESs. Density, viscosity, and melting point of these functional iDESs were measured, as well as flow activation energy was calculated. CO_2 absorptions were measured under different capture temperatures and partial pressures of CO_2, especially at high capture temperature or low partial pressure of CO_2, which indicated the chemical interactions. Thermodynamic properties of CO_2 absorbed in pyridinolate-containing functional iDESs, such as the change of molar Gibbs free energy of the reaction ($\Delta_r G^\theta$m), the change of molar enthalpy of the reaction ($\Delta_r H^\theta$m), and the change of molar entropy of the reaction ($\Delta_r S^\theta$m), were analyzed, and the $\Delta_r H^\theta$m was predominant for the favorable 1:1 chemisorption of CO_2. The performance of CO_2 conversion with 2-aminobenzonitrile and its derivatives using these pyridinolate-containing DESs as the green solvents, sorbents, and catalysts was also investigated, and excellent isolated yield of up to 97.1% quinazoline-2,4(1*H*,3*H*)-dione and its derivatives at mild conditions could be obtained with only 0.25 equiv. $[N_{2222}][4\text{-PyO}]$/DMSO (1:4) through "simultaneous CO_2 activation and substrate activation" reaction mechanism. To the best of our knowledge, these are the first examples of tuning functional iDESs for capture and

Table 5
CO_2 conversion with different substituted ABN [a].

Entry	Substrate	Product	Isolated yield (%)
1	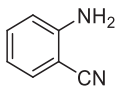	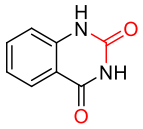	92.9
2	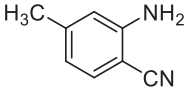	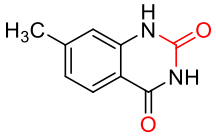	73.0
3	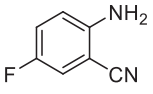	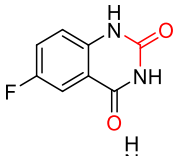	97.1
4	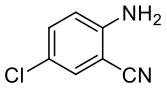	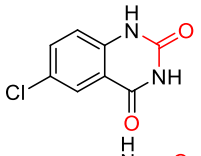	91.4
5	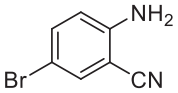	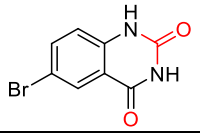	90.9

[a] Reaction conditions: $[N_{2222}][4\text{-PyO}]$/DMSO (1:4) 0.25 mmol, substrate 1 mmol, 50 °C, 24 h, 1 bar CO_2 balloon.

transformation of CO_2 to quinazoline-2,4-(1*H*,3*H*)-dione and its derivatives with only 0.25 equiv. DES. We believe that this strategy could open a door to achieving high efficiency of capture and conversion of gases such as NO_x, SO_2, H_2S, and CO_2 by functional DESs.

CRediT authorship contribution statement

Guokai Cui: Supervision, Conceptualization, Project administration, Funding acquisition, Investigation, Writing – original draft, Writing – review & editing. **Yisha Xu:** Investigation, Data curation, Visualization, Writing – review & editing. **Daqing Hu:** Formal analysis. **Ying Zhou:** Resources, Supervision. **Chunliang Ge:** Resources, Formal analysis. **Huayan Liu:** Methodology, Formal analysis. **Wenyang Fan:** Formal analysis. **Zekai Zhang:** Validation. **Biao Chen:** Validation. **Quanli Ke:** Formal analysis, Funding acquisition. **Yaoji Chen:** Validation. **Bing Zhou:** Formal analysis. **Wei Zhang:** Resources, Validation. **Ruina Zhang:** Data curation, Visualization. **Hanfeng Lu:** Conceptualization, Project administration, Resources, Funding acquisition.

Declaration of Competing Interest

The authors declare that they have no known competing financial interests or personal relationships that could have appeared to influence the work reported in this paper.

Data availability

Data will be made available on request.

Acknowledgements

This work was supported by the National Natural Science Foundation of China (22078294 and 22208300), the Zhejiang Provincial Natural Science Foundation of China (LZ21E080001), Key Research and Development Project in Zhejiang Province (2023C03127), National Key Research and Development Program of China (2022YFC3702003), and the Zhejiang Tiandi Environmental Protection Technology Co., Ltd. “Development of Ionic Liquid Absorbents for Carbon Dioxide Capture with Green and Low Energy Consumption” Technology Project (No. TD-KJ-22-007-W001).

Appendix A. Supplementary data

Supplementary data to this article can be found online at https://doi.org/10.1016/j.cej.2023.143991.

References

[1] Q. Lin, X. Zhang, T. Wang, C. Zheng, X. Gao, Technical Perspective of Carbon Capture, Utilization, and Storage, Engineering 14 (2022) 27–32, https://doi.org/10.1016/j.eng.2021.12.013.
[2] W. Gao, S. Liang, R. Wang, Q. Jiang, Y. Zhang, Q. Zheng, B. Xie, C.Y. Toe, X. Zhu, J. Wang, L. Huang, Y. Gao, Z. Wang, C. Jo, Q. Wang, L. Wang, Y. Liu, B. Louis, J. Scott, A.-C. Roger, R. Amal, H. He, S.-E. Park, Industrial carbon dioxide capture and utilization: state of the art and future challenges, Chem. Soc. Rev. 49 (23) (2020) 8584–8686, https://doi.org/10.1039/D0CS00025F.
[3] H. Wang, Y. Wu, Y. Zhao, Z. Liu, Recent Progress on Ionic Liquid-Mediated CO2 Conversion, Acta Phys-Chim Sin 37 (5) (2021), https://doi.org/10.3866/PKU.WHXB202010022.
[4] C. Kim, C.-J. Yoo, H.-S. Oh, B.K. Min, U. Lee, Review of carbon dioxide utilization technologies and their potential for industrial application, J. CO2 Util. 65 (2022), 102239, https://doi.org/10.1016/j.jcou.2022.102239.
[5] Y. Chen, T. Mu, Conversion of CO2 to value-added products mediated by ionic liquids, Green Chem. 21 (10) (2019) 2544–2574, https://doi.org/10.1039/C9GC00827F.
[6] D. Gheidari, M. Mehrdad, S. Maleki, The quinazoline-2,4(1H,3H)-diones skeleton: A key intermediate in drug synthesis, Sustainable Chem. Pharm. 27 (2022), 100696, https://doi.org/10.1016/j.scp.2022.100696.
[7] R. Zhang, D. Hu, Y. Zhou, C. Ge, H. Liu, W. Fan, L. Li, B. Chen, Y. Cheng, Y. Chen, W. Zhang, G. Cui, H. Lu, Tuning Ionic Liquid-Based Catalysts for CO2 Conversion into Quinazoline-2,4(1H,3H)-diones, Molecules 28 (3) (2023) 1024, https://doi.org/10.3390/molecules28031024.
[8] Y. Liu, Z. Dai, Z. Zhang, S. Zeng, F. Li, X. Zhang, Y. Nie, L. Zhang, S. Zhang, X. Ji, Ionic liquids/deep eutectic solvents for CO2 capture: Reviewing and evaluating, Green Energy Environ. 6 (3) (2021) 314–328, https://doi.org/10.1016/j.gee.2020.11.024.
[9] B.B. Hansen, S. Spittle, B. Chen, D. Poe, Y. Zhang, J.M. Klein, A. Horton, L. Adhikari, T. Zelovich, B.W. Doherty, B. Gurkan, E.J. Maginn, A. Ragauskas, M. Dadmun, T.A. Zawodzinski, G.A. Baker, M.E. Tuckerman, R.F. Savinell, J. R. Sangoro, Deep Eutectic Solvents: A Review of Fundamentals and Applications, Chem. Rev. 121 (3) (2021) 1232–1285, https://doi.org/10.1021/acs.chemrev.0c00385.
[10] R. Zhang, Q. Ke, Z. Zhang, B. Zhou, G. Cui, H. Lu, Tuning Functionalized Ionic Liquids for CO_2 Capture, Int. J. Mol. Sci. 23 (19) (2022) 11401, https://doi.org/10.3390/ijms231911401.
[11] Y. Chen, T. Mu, Revisiting greenness of ionic liquids and deep eutectic solvents, Green Chem. Eng. 2 (2) (2021) 174–186, https://doi.org/10.1016/j.gce.2021.01.004.
[12] Y. Zhao, B. Yu, Z. Yang, H. Zhang, L. Hao, X. Gao, Z. Liu, A Protic Ionic Liquid Catalyzes CO_2 Conversion at Atmospheric Pressure and Room Temperature: Synthesis of Quinazoline-2,4(1*H*,3*H*)-diones, Angew. Chem., Int. Ed. 53(23) (2014) 5922-5925. https://doi.org/10.1002/anie.201400521.
[13] W. Lu, J. Ma, J. Hu, J. Song, Z. Zhang, G. Yang, B. Han, Efficient synthesis of quinazoline-2,4(1*H*,3*H*)-diones from CO_2 using ionic liquids as a dual solvent–catalyst at atmospheric pressure, Green Chem. 16 (1) (2014) 221–225, https://doi.org/10.1039/C3GC41467A.
[14] M. Hulla, S.M.A. Chamam, G. Laurenczy, S. Das, P.J. Dyson, Delineating the Mechanism of Ionic Liquids in the Synthesis of Quinazoline-2,4(1*H*,3*H*)-dione from 2-Aminobenzonitrile and CO_2, Angew. Chem., Int. Ed. 56(35) (2017) 10559-10563. https://doi.org/10.1002/anie.201705438.
[15] G. Shi, K. Chen, Y. Wang, H. Li, C. Wang, Highly Efficient Synthesis of Quinazoline-2,4(1H,3H)-diones from CO2 by Hydroxyl Functionalized Aprotic Ionic Liquids, ACS Sustainable Chem. Eng. 6 (5) (2018) 5760–5765, https://doi.org/10.1021/acssuschemeng.8b01109.
[16] F. Liu, R. Ping, Y. Gu, P. Zhao, B. Liu, J. Gao, M. Liu, Efficient One Pot Capture and Conversion of CO_2 into Quinazoline-2,4(1*H*,3*H*)-diones Using Triazolium-Based Ionic Liquids, ACS Sustainable Chem. Eng. 8 (7) (2020) 2910–2918, https://doi.org/10.1021/acssuschemeng.9b07242.
[17] F. Liu, R. Ping, P. Zhao, Y. Gu, J. Gao, M. Liu, Succinimide-Based Ionic Liquids: An Efficient and Versatile Platform for Transformation of CO2 into Quinazoline-2,4(1H,3H)-diones under Mild and Solvent-Free Conditions, ACS Sustainable Chem. Eng. 7 (15) (2019) 13517–13522, https://doi.org/10.1021/acssuschemeng.9b03154.
[18] T. Chen, Y. Zhang, Y. Xu, Efficient Synthesis of Quinazoline-2,4(1*H*,3*H*)-dione via Simultaneous Activated CO_2 and 2-Aminobenzonitrile by 1-Methylhydantoin Anion-Functionalized Ionic Liquid through the Multiple-Site Cooperative Interactions, ACS Sustainable Chem. Eng. 10 (32) (2022) 10699–10711, https://doi.org/10.1021/acssuschemeng.2c03249.
[19] R. Ping, P. Zhao, Q. Zhang, G. Zhang, F. Liu, M. Liu, Catalytic Conversion of CO2 from Simulated Flue Gases with Aminophenol-Based Protic Ionic Liquids to Produce Quinazoline-2,4(1H,3H)-diones under Mild Conditions, ACS Sustainable Chem. Eng. 9 (14) (2021) 5240–5249, https://doi.org/10.1021/acssuschemeng.1c01466.
[20] H. Zhang, J.M. Vicent-Luna, S. Tao, S. Calero, R.J. Jiménez Riobóo, M.L. Ferrer, F. del Monte, M.C. Gutiérrez, Transitioning from Ionic Liquids to Deep Eutectic Solvents, ACS Sustainable Chem. Eng. 10 (3) (2022) 1232–1245.
[21] N. Ismail, J. Pan, M. Rahmati, Q. Wang, D. Bouyer, M. Khayet, Z. Cui, N. Tavajohi, Non-ionic deep eutectic solvents for membrane formation, J. Membr. Sci. 646 (2022), 120238, https://doi.org/10.1016/j.memsci.2021.120238.
[22] H. Zhao, Z. Wang, C. Zhang, S. Di, P. Qi, Z. Wang, Z. Liu, H. Xu, J. Wang, X. Wang, Phenolic-based non-ionic deep eutectic solvent for rapid determination of water soluble neonicotinoid insecticides in tea infusion, Food Chem. 416 (2023), 135737, https://doi.org/10.1016/j.foodchem.2023.135737.
[23] D.O. Abranches, M.A.R. Martins, L.P. Silva, N. Schaeffer, S.P. Pinho, J.A. P. Coutinho, Phenolic hydrogen bond donors in the formation of non-ionic deep eutectic solvents: the quest for type V DES, Chem. Commun. 55 (69) (2019) 10253–10256, https://doi.org/10.1039/C9CC04846D.
[24] O.V. Kazarina, V.N. Agieienko, A.N. Petukhov, A.V. Vorotyntsev, M.E. Atlaskina, A. A. Atlaskin, S.S. Kryuchkov, A.N. Markov, A.V. Nyuchev, I.V. Vorotyntsev, Deep Eutectic Solvents Composed of Urea and New Salts of a Choline Family for Efficient Ammonia Absorption, J. Chem. Eng. Data 67 (1) (2022) 138–150, https://doi.org/10.1021/acs.jced.1c00684.
[25] Y. Zhong, J. Wu, H. Kang, R. Liu, Choline hydroxide based deep eutectic solvent for dissolving cellulose, Green Chem. 24 (6) (2022) 2464–2475, https://doi.org/10.1039/D1GC04130D.
[26] I. Adeyemi, M.R.M. Abu-Zahra, I.M. AlNashef, Physicochemical properties of alkanolamine-choline chloride deep eutectic solvents: Measurements, group contribution and artificial intelligence prediction techniques, J. Mol. Liq. 256 (2018) 581–590, https://doi.org/10.1016/j.molliq.2018.02.085.
[27] S.K. Shukla, J.-P. Mikkola, Intermolecular interactions upon carbon dioxide capture in deep-eutectic solvents, PCCP 20 (38) (2018) 24591–24601, https://doi.org/10.1039/c8cp03724h.
[28] G. Cui, K. Jiang, H. Liu, Y. Zhou, Z. Zhang, R. Zhang, H. Lu, Highly efficient CO removal by active cuprous-based ternary deep eutectic solvents [HDEEA][Cl] + CuCl + EG, Sep. Purif. Technol. 274 (2021), 118985.

[29] H. Sang, L. Su, W. Han, F. Si, W. Yue, X. Zhou, Z. Peng, H. Fu, Basicity-controlled DBN-based deep eutectic solvents for efficient carbon dioxide capture, J. CO2 Util. 65 (2022), 102201, https://doi.org/10.1016/j.jcou.2022.102201.
[30] C. Fan, L. Wen, Y. Shan, Y. Shan, X. Cao, Why do ammonium salt/phenol-based deep eutectic solvents show low viscosity? Arab. J. Chem. 15 (1) (2022), 103512 https://doi.org/10.1016/j.arabjc.2021.103512.
[31] Y. Liu, Z. Cao, Z. Zhou, A. Zhou, Imidazolium-based deep eutectic solvents as multifunctional catalysts for multisite synergistic activation of epoxides and ambient synthesis of cyclic carbonates, J. CO2 Util. 53 (2021), 101717, https://doi.org/10.1016/j.jcou.2021.101717.
[32] M. Gao, Y. Hou, Q. Zhang, Y. Sun, S. Ren, W. Wu, Absorption of SO2 in Simulated Flue Gas by Functional Deep Eutectic Solvents Based on Imidazole and H2O with High Mass Capacities, Energy Fuels 34 (4) (2020) 4754–4760, https://doi.org/10.1021/acs.energyfuels.0c00057.
[33] M. Sajjadur Rahman, J. Kyeremateng, M. Saha, S. Asare, N. Uddin, M.A. Halim, D. E. Raynie, Evaluation of the experimental and computed properties of choline chloride-water formulated deep eutectic solvents, J. Mol. Liq. 350 (2022), 118520, https://doi.org/10.1016/j.molliq.2022.118520.
[34] J. Cao, C. Wang, L. Shi, Y. Cheng, H. Hu, B. Zeng, F. Zhao, Water based-deep eutectic solvent for ultrasound-assisted liquid–liquid microextraction of parabens in edible oil, Food Chem. 383 (2022), 132586, https://doi.org/10.1016/j.foodchem.2022.132586.
[35] D. Yang, S. Zhang, D.-E. Jiang, Efficient Absorption of SO2 by Deep Eutectic Solvents Formed by Biobased Aprotic Organic Compound Succinonitrile and 1-Ethyl-3-methylimidazolium Chloride, ACS Sustainable Chem. Eng. 7 (10) (2019) 9086–9091, https://doi.org/10.1021/acssuschemeng.9b00851.
[36] D. Yang, S. Zhang, X.-G. Sun, D.-E. Jiang, S. Dai, Deep eutectic solvents formed by quaternary ammonium salts and aprotic organic compound succinonitrile, J. Mol. Liq. 274 (2019) 414–417, https://doi.org/10.1016/j.molliq.2018.10.150.
[37] Z. Hu, F. Xian, Z. Guo, C. Lu, X. Du, X. Cheng, S. Zhang, S. Dong, G. Cui, L. Chen, Nonflammable Nitrile Deep Eutectic Electrolyte Enables High-Voltage Lithium Metal Batteries, Chem. Mater. 32 (8) (2020) 3405–3413, https://doi.org/10.1021/acs.chemmater.9b05003.
[38] I.A. Rather, R. Ali, A Facile Deep Eutectic Solvent (DES) Mediated Green Approach for the Synthesis of Fluorescein and Phenolphthalein Dyes, ChemistrySelect 8 (12) (2023) e202300749.
[39] D.-J. Tao, F. Qu, Z.-M. Li, Y. Zhou, Promoted absorption of CO at high temperature by cuprous-based ternary deep eutectic solvents, AIChE J 67 (2) (2021) e17106.
[40] G. Cui, J. Liu, S. Lyu, H. Wang, Z. Li, R. Zhang, J. Wang, SO2 absorption in highly efficient chemical solvent AChBr + Gly compared with physical solvent ChBr + Gly, J. Mol. Liq. 330 (2021), 115650, https://doi.org/10.1016/j.molliq.2021.115650.
[41] F. Li, A. Laaksonen, X. Zhang, X. Ji, Rotten Eggs Revaluated: Ionic Liquids and Deep Eutectic Solvents for Removal and Utilization of Hydrogen Sulfide, Ind. Eng. Chem. Res. 61 (7) (2022) 2643–2671, https://doi.org/10.1021/acs.iecr.1c04142.
[42] Y. Chen, X. Han, Z. Liu, D. Yu, W. Guo, T. Mu, Capture of Toxic Gases by Deep Eutectic Solvents, ACS Sustainable Chem. Eng. 8 (14) (2020) 5410–5430, https://doi.org/10.1021/acssuschemeng.0c01493.
[43] L. Peng, M. Shi, Y. Pan, Z. Tu, X. Hu, X. Zhang, Y. Wu, Ultrahigh carbon monoxide capture by novel protic cuprous-functionalized dicationic ionic liquids through complexation interactions, Chem. Eng. J. 451 (2023), 138519, https://doi.org/10.1016/j.cej.2022.138519.
[44] Z. Yuan, H. Liu, W.F. Yong, Q. She, J. Esteban, Status and advances of deep eutectic solvents for metal separation and recovery, Green Chem. 24 (5) (2022) 1895–1929, https://doi.org/10.1039/D1GC03851F.
[45] M.F. Lanjwani, M. Tuzen, M.Y. Khuhawar, M.R. Afshar Mogaddam, M. A. Farajzadeh, Deep Eutectic Solvents for Extraction and Preconcentration of Organic and Inorganic Species in Water and Food Samples: A Review, Crit. Rev. Anal. Chem. (2022) 1–14, https://doi.org/10.1080/10408347.2022.2111655.
[46] M. Shi, W. Xiong, Z. Tu, X. Zhang, X. Hu, Y. Wu, Task-specific deep eutectic solvents for the highly efficient and selective separation of H2S, Sep. Purif. Technol. 276 (2021), 119357, https://doi.org/10.1016/j.seppur.2021.119357.
[47] C.L. Boldrini, A.F. Quivelli, N. Manfredi, V. Capriati, A. Abbotto, Deep Eutectic Solvents in Solar Energy Technologies 27 (3) (2022) 709, https://doi.org/10.3390/molecules27030709.
[48] S. Azmi, M.F. Koudahi, E. Frackowiak, Reline deep eutectic solvent as a green electrolyte for electrochemical energy storage applications, Energy Environ. Sci. 15 (3) (2022) 1156–1171, https://doi.org/10.1039/D1EE02920G.
[49] R. Abro, N. Kiran, S. Ahmed, A. Muhammad, A.S. Jatoi, S.A. Mazari, U. Salma, N. V. Plechkova, Extractive desulfurization of fuel oils using deep eutectic solvents – A comprehensive review, J. Environ. Chem. Eng. 10 (3) (2022), 107369, https://doi.org/10.1016/j.jece.2022.107369.
[50] P. Zhang, W. Xiong, M. Shi, Z. Tu, X. Hu, X. Zhang, Y. Wu, Natural deep eutectic solvent-based gels with multi-site interaction mechanism for selective membrane separation of SO2 from N2 and CO2, Chem. Eng. J. 438 (2022), 135626, https://doi.org/10.1016/j.cej.2022.135626.
[51] G. Cui, J. Liu, S. Lyu, H. Wang, Z. Li, J. Wang, Efficient and Reversible SO_2 Absorption by Environmentally Friendly Task-Specific Deep Eutectic Solvents of PPZBr + Gly, ACS Sustainable Chem. Eng. 7 (16) (2019) 14236–14246, https://doi.org/10.1021/acssuschemeng.9b03245.
[52] I.B. Qader, K. Prasad, Recent Developments on Ionic Liquids and Deep Eutectic Solvents for Drug Delivery Applications, Pharm. Res. 39 (10) (2022) 2367–2377.
[53] X. Yang, Q. Zou, T. Zhao, P. Chen, Z. Liu, F. Liu, Q. Lin, Deep Eutectic Solvents as Efficient Catalysts for Fixation of CO2 to Cyclic Carbonates at Ambient Temperature and Pressure through Synergetic Catalysis, ACS Sustainable Chem. Eng. 9 (31) (2021) 10437–10443, https://doi.org/10.1021/acssuschemeng.1c03187.
[54] K.K. Maniam, S. Paul, Ionic Liquids and Deep Eutectic Solvents for CO2 Conversion Technologies—A Review, Materials 14 (16) (2021) 4519, https://doi.org/10.3390/ma14164519.
[55] D. Mańka, A. Siewniak, Deep Eutectic Solvents as Catalysts for Cyclic Carbonates Synthesis from CO2 and Epoxides, Molecules 27 (24) (2022) 9006, https://doi.org/10.3390/molecules27249006.
[56] I. Dindarloo Inaloo, S. Majnooni, Carbon dioxide utilization in the efficient synthesis of carbamates by deep eutectic solvents (DES) as green and attractive solvent/catalyst systems, New J. Chem. 43 (28) (2019) 11275–11281.
[57] Y. Xu, R. Zhang, Y. Zhou, D. Hu, C. Ge, W. Fan, B. Chen, Y. Chen, W. Zhang, H. Liu, G. Cui, H. Lu, Tuning ionic liquid-based functional deep eutectic solvents and other functional mixtures for CO2 capture, Chem. Eng. J. 463 (2023), 142298, https://doi.org/10.1016/j.cej.2023.142298.
[58] X. Luo, Y. Guo, F. Ding, H. Zhao, G. Cui, H. Li, C. Wang, Significant Improvements in CO_2 Capture by Pyridine-Containing Anion-Functionalized Ionic Liquids through Multiple-Site Cooperative Interactions, Angew. Chem., Int. Ed. 53(27) (2014) 7053-7057. https://doi.org/10.1002/anie.201400957.
[59] G. Cui, M. Lv, D. Yang, Efficient CO_2 absorption by azolide-based deep eutectic solvents, Chem. Commun. 55 (10) (2019) 1426–1429, https://doi.org/10.1039/C8CC10085C.
[60] Z. Wang, Z. Wang, X. Huang, D. Yang, C. Wu, J. Chen, Deep eutectic solvents composed of bio-phenol-derived superbase ionic liquids and ethylene glycol for CO2 capture, Chem. Commun. 58 (13) (2022) 2160–2163, https://doi.org/10.1039/D1CC06856C.
[61] M.J. Frisch, G.W. Trucks, H.B. Schlegel, G.E. Scuseria, M.A. Robb, J.R. Cheeseman, G. Scalmani, V. Barone, G.A. Petersson, H. Nakatsuji, X. Li, M. Caricato, A.V. Marenich, J. Bloino, B.G. Janesko, R. Gomperts, B. Mennucci, H.P. Hratchian, J.V. Ortiz, A.F. Izmaylov, J.L. Sonnenberg, D. Williams-Young, F. Ding, F. Lipparini, F. Egidi, J. Goings, B. Peng, A. Petrone, T. Henderson, D. Ranasinghe, V.G. Zakrzewski, J. Gao, N. Rega, G. Zheng, W. Liang, M. Hada, M. Ehara, K. Toyota, R. Fukuda, J. Hasegawa, M. Ishida, T. Nakajima, Y. Honda, O. Kitao, H. Nakai, T. Vreven, K. Throssell, J. Montgomery, J. A., J.E. Peralta, F. Ogliaro, M.J. Bearpark, J.J. Heyd, E.N. Brothers, K.N. Kudin, V.N. Staroverov, T.A. Keith, R. Kobayashi, J. Normand, K. Raghavachari, A.P. Rendell, J.C. Burant, S.S. Iyengar, J. Tomasi, M. Cossi, J.M. Millam, M. Klene, C. Adamo, R. Cammi, J.W. Ochterski, R.L. Martin, K. Morokuma, O. Farkas, J.B. Foresman, D.J. Fox, Gaussian 16 (Revision C.01), Gaussian, Inc., Wallingford CT, 2019.
[62] A. Bondi, van der Waals Volumes and Radii, J. Phys. Chem. 68 (3) (1964) 441–451, https://doi.org/10.1021/j100785a001.